

Real-Time PMU-Assisted Wide-Area Oscillation Damping using Active Load Control

GUÐRÚN MARGRÉT JÓNSDÓTTIR



KTH Electrical Engineering

Master's Degree Project
Stockholm, Sweden September 2015



Real-Time PMU-Assisted Wide-Area Oscillation Damping using Active Load Control

GUÐRÚN MARGRÉT JÓNSDÓTTIR

Master's Thesis at SmarTS Lab, Electric Power Systems, KTH
Supervisor: Muhammad Shoib Almas, Maxime Baudette & Magni Þór Pálsson
Examiner: Luigi Vanfretti

TRITA-EE 2015:60

Acknowledgements

I have so many people to thank, but at the top of my list is Almas, my supervisor. He is an inspiration to me and was there with me through every step of my thesis. We have spent countless hours talking about my thesis work, Frozen and everything there in between. He does drive me crazy sometimes because he is almost never on time, but he makes up for it by having the biggest heart and he puts a smile on my face every time I meet him. To you Almas I say stay blessed and keep smiling, thank you for everything.

Thank you so much to Luigi for taking a chance on me. When I look back on these two years that I have known you, I feel so grateful and blessed for all the amazing opportunities I have had because of you. I am so proud to be your student and to have you as a friend. You make me want to do better and be better. Hugs!

Thank you Maxime for giving me advice about everything no matter if I care for it or not and thank you for being a friend. You have been my go to guy throughout this whole project and I am so grateful to you. I want to give special shout out to my lab partner Ravi who has made sure I didn't lose my mind and for celebrating with me when I solved my problems, no matter how small they were. I am so grateful for being a part of team SmarTS Lab and I say thank you to all my team members for your love and support.

I would not be where I am today without my family. They are everything to me and my biggest cheerleaders. Til mömmu, pabba og Auðar ég elskar ykkur, þetta er fyrir ykkur. Thank you Unnar for being there with me through the ups and the downs, for listening and for making me laugh when I needed to. You are my rock.

To all the people I have met here at KTH over the last two years that have made my stay here memorable and filled with good food, thank you. Hugs and kisses to you all.

A big thank you to Nordic Energy Research that has financially supported this master thesis through the Strong²rid project. Last but not least, thank you to Landsnet, the Icelandic Power System Operator for all their support and help. I am extremely thankful that I got the opportunity to work on this interesting project in co-operation with them. An extra thank you to Magni, my contact at Landsnet who is also the reason I decided to study electric power engineering.

Abstract

The Icelandic network is a unique system, characterised by heavy loads concentrated in two main areas, in the southwest and in the east of the island. These two areas are connected together through a weak tie-line resulting in frequent and strong inter-area oscillations. These oscillations cause the transmission limit of the tie-line to be exceeded and the system has to be separated into islands. Conventional means for stabilization, such as the use of PSSs in generators and supplementary damping controls in FACTS, have been used to their full capacity and thus new options are being explored to tackle the recurring issues. There is potential in exploiting large industrial loads, like aluminium smelters, for enhancing system stability during these particular stressful operating conditions.

In this thesis, two active load control algorithms are developed for oscillation damping. Synchrophasor measurements are used as input signals for these algorithms. The algorithms can use either local or remote synchrophasor measurements. The algorithms are then tested using different input signals (voltage magnitude, current magnitude and voltage phase angle difference, etc.) to find the most effective input signal. The algorithms are tested in a Real-Time Hardware-in-the-Loop (RT-HIL) environment where the load control algorithms are deployed on an external controller and fed by synchrophasors from Phasor Measurement Units (PMUs).

By using the RT-HIL simulation approach, the thesis concludes that active-load control algorithms that utilize either local and/or remote measurements, can be exploited to provide adequate damping for inter-area oscillations. In addition, this thesis provides recommendations for generic hardware prototype design, development, testing and performance assessment of real-time PMU-assisted controls.

Referat

Det isländska kraftsystemet är unikt i det att tunga laster är koncentrerade till två huvudsakliga områden, den sydvästra och den östra delen av ön. Dessa två områden är sammankopplade med en förhållandevis svag kraftledning vilket ofta ger upphov till starka oscillationer mellan de olika områdena, på engelska: inter-area oscillations. Dessa oscillationer gör att överföringskapaciteten i korridoren överskrids och kraftsystemet måste separeras till två system i ö-drift. Konventionella metoder för stabilisering, som till exempel PSS-regulatorer i generatorerna och dämpningsregulatorer i FACTS-komponenter är redan utnyttjade till fullo och därfor undersöks nya alternativ för att hantera dessa återkommande problem. Det finns en potential i att utnyttja stora industriella laster, så som aluminiумsmältverk, för att förbättra systemets stabilitet i dessa väldigt stressade driftsituationer.

I detta examensarbete har två regleralgoritmer utvecklats för att styra lasternas aktiva effekt så att oscillationerna dämpas. Synkroniserade fasvektorer används som insignal för dessa algoritmer. Algoritmerna kan använda antingen lokala mätningar eller mätningar från andra delar av systemet. Algoritmerna är testade med olika insignaler (t. ex. spänningsmagnitud, strömmagnitud, och fasvinkelskillnad mellan spänningfasvektorer) för att finna den mest effektiva insignalen. Algoritmerna testades också i en testbädd för realtidssimulering med hårdvara i en återkoppling, Real-Time Hardware-in-the-Loop (RT-HIL), där algoritmerna implementerades i ett externt styrsystem som matades med fasvektordata från Phasor Measurement Units (PMU:er).

Genom att använda RT-HIL kan detta examensarbete konkludera att reglersystem för styrning av lasternas aktiva effekt genom lokala och/eller fjärr-mätningar kan användas för att ge tillräcklig dämpning vid inter-area oscillations. Dessutom ger examensarbetet allmänna rekommendationer för konstruktion, utveckling, testning och effektivitetsutvärderingar av hårdvaruprototyper för realtid-regulatorer som använder PMU-data.

Contents

1	Introduction	3
1.1	Background	3
1.2	Objectives	5
1.2.1	General Objectives	5
1.2.2	Specific Objectives	6
1.2.3	Assumptions and Limitations of the Project	6
1.3	Thesis Outline	7
2	Background	9
2.1	Power System Oscillations	9
2.2	Power System Oscillation Damping	11
2.2.1	Means for damping of inter-area oscillations	11
2.2.2	Conventional Control Approach	12
2.2.3	Phasor-Based Control Approach	12
2.3	Wide-Area Monitoring and Control	13
2.3.1	Phasors and Synchrophasors	13
2.3.2	PMUs and PDCs	14
2.3.3	Laboratory Infrastructure for Implementing and Testing	16
3	Load Control Algorithm: Design and Testing	19
3.1	The Test Power System Model	19
3.2	The Load Control Algorithm	20
3.2.1	Phasor POD	20
3.2.2	Algorithm 1	20
3.2.3	Algorithm 2	21
3.3	Algorithm Testing Approach	22
3.4	Testing Preparation	22
3.4.1	Preparation of the Simulink Model for Offline Simulation	23
3.4.2	Modifications for Real-Time Simulation	23
3.4.3	Hardware-in-the-Loop Execution	25
3.5	Algorithm Refinement	29
4	Tests and Results	33

4.1	Active Power as Input Signal	34
4.1.1	RT-SIL	34
4.1.2	RT-HIL	34
4.1.3	Comparing RT-SIL and RT-HIL	35
4.2	Signal Selection	36
4.2.1	RT-SIL	37
4.2.2	RT-HIL	39
4.3	Further Analysis	40
4.3.1	Latency Analysis	40
4.3.2	Scaling Analysis	42
4.3.3	Noise Analysis	43
5	Closure	45
5.1	Summary	45
5.2	Future Work	46
Bibliography		47
Appendices		50
A Test Power System Model Parameters		51
B Results for Scenario 2		53
C Figures of Setup		55
D New Approach for Determining the Amount of Load Change		57

Symbols and abbreviations

AC	Alternating Current
AI/O	Analog Input/Output
cRIO	Compact Reconfigurable Input/Output
DC	Direct Current
DR	Decay Ratio
FACTS	Flexible AC Transmission Systems
FPGA	Field-Programmable Gate Array
GPS	Global Positioning System
HIL	Hardware-in-the-Loop
HVDC	High-Voltage Direct Current
IP	Internet Protocol
LP	Low Pass
MIL	Model-in-the-Loop
NI	National Instruments
PDC	Phasor Data Concentrator
PMU	Phasor Measurement Unit
POD	Power Oscillation Damper
PSS	Power System Stabilizer
RLS	Recursive least squares
RMS	Root Mean Square
ROCOF	Rate-of-Change-of-Frequency
RT	Real-Time
S ³ DK	Statnett's Synchrophasor Software Development Kit
SEL	Schweitzer Engineering Laboratories
SIL	Software-in-the-Loop
SVC	Static VAR Compensator
TCP	Transmission Control Protocol
TSO	Transmission System Operator
UDP	User Datagram Protocol
TCSC	Thyristor Controlled Series Capacitor
UTC	Coordinated Universal Time
VI	Virtual Instrument (LabVIEW™Code)
WACS	Wide-Area Control System
WAMPAC	Wide-Area Monitoring Protection and Control

Chapter 1

Introduction

1.1 Background

The Icelandic transmission system consists of two meshed 220 kV networks, located in the south-western and in the eastern part of the island. The whole system is interconnected through two 132 kV transmission lines that are over 1000 km long, thus, forming a ring around the island [1]. This interconnection was built about 30 years ago and was a big step forward at the time, allowing new power plants to be built and increasing the electric security throughout the country. However, because of environmental concerns and an increasing opposition to building transmission lines, no new interconnections between the two areas have been built ever since. Thus, these lines are, today, largely fatigued and often overloaded. In 2013, the national Transmission System Operator (TSO), Landsnet, estimated a limitation of 100 MW of active power transfer between the south-western and the eastern part of the island as illustrated on Fig. 1.1 [2].

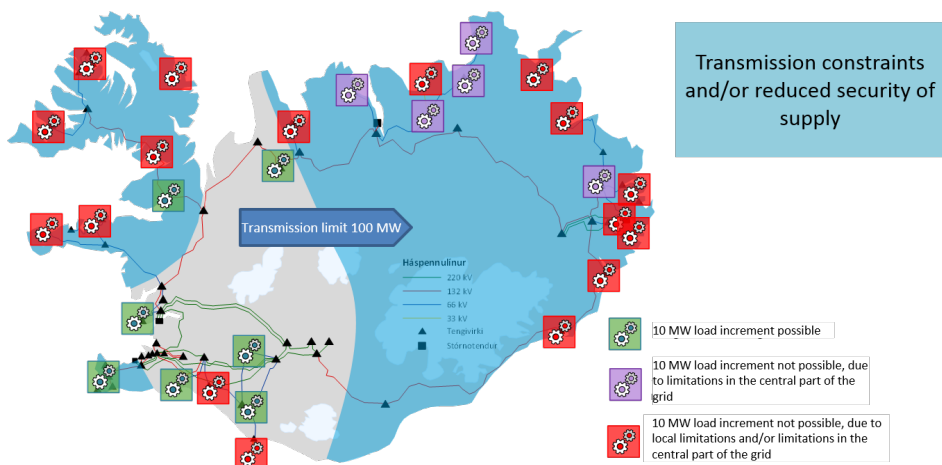


Figure 1.1: The Icelandic power system indicating the 100 MW transmission limit between the southwest and the east.

When large generation and load clusters are inter-connected by a weak tie-line or long distance corridors small disturbances may cause generator groups in the interconnected areas to start oscillating against each other. These inter-area oscillations may lead to major blackouts if not sufficiently damped [3]. In the Icelandic network, inter-area oscillations occur often causing the machines in the northern and eastern part of the system to oscillate in anti-phase with the south-western 220 kV network [1]. These oscillations often cause the transmission limit in Fig. 1.1 (100 MW) to be reached, resulting in a system separation to preserve the stability in the two areas.

In 2007 a Wide-Area Monitoring System (WAMS) was installed in the Icelandic power system to monitor the stability of the 132 kV ring. PhasorPoint from Psymetrix is used [4]. Psymetrix is a company owned by Alstom offering WAMS products and services. Phasor Measurement Units (PMUs) were installed throughout the network, their locations can be seen in Fig. 1.2 [5]. The WAMS system has provided valuable information during large system faults, in particular the ones resulting in the islanding of the systems. The difference in angle and speed between the two areas has been used to generate a tripping signal in the south-western part of the grid. This is a part of Landsnets Wide-Area Defence Scheme [4]. Landsnet also uses PSSs, load shedding and other measures to keep the system stable [6].

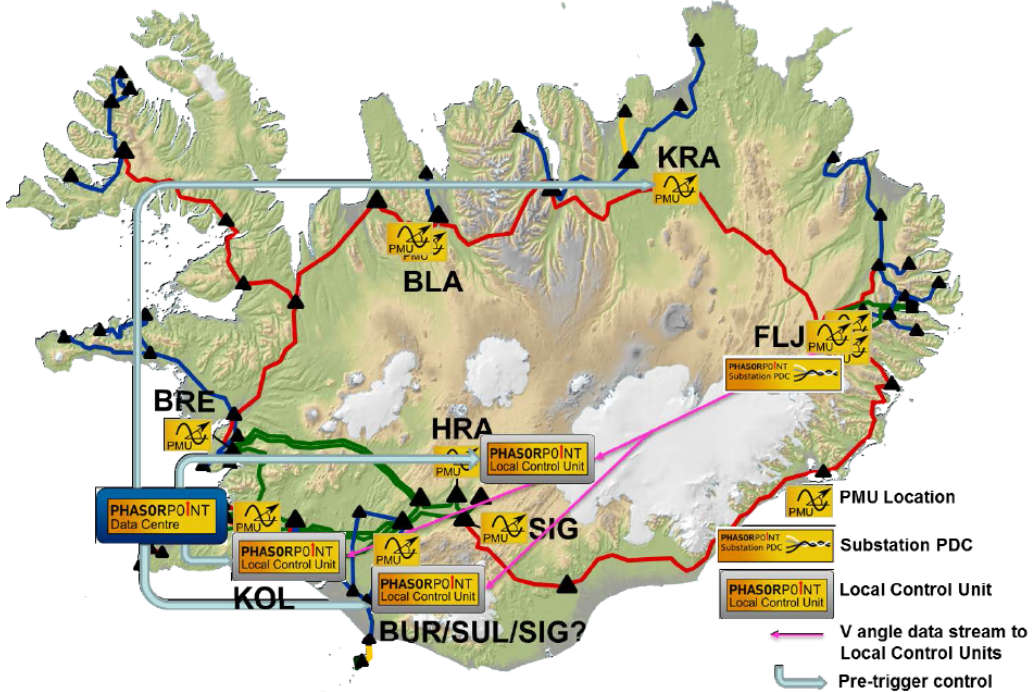


Figure 1.2: Architecture of the WAMS system and placement of PMUs and PDCs in the Icelandic power system.

Traditionally, electric power systems have relied on generators and transmission equipment for maintaining system stability. Additionally, load shedding schemes

1.2. OBJECTIVES

have been used to prevent under-frequency operation or to avoid blackouts. However, there is a potential to use actively controlled loads for system stability enhancement during stressed network operation conditions. The use of active load control was discussed as early as in 1968 [7] but at that time it was considered economically infeasible. In more recent years, the importance of giving the load a more active role to stabilize the system has been identified and the interest in load control has been renewed [8].

About 80 % of the total electricity consumption in Iceland comes from industrial loads [9], see Fig. 1.3. The reducible load shown in Fig. 1.3 is load that currently can be shed by Landsnet as a measure to keep the system stable. The largest part of the industrial load is comprised of aluminium smelters [10]. This context helped originating an idea at the Icelandic TSO, to control the load of the aluminium smelters using WACS when the grid is subjected to faults. The proposal was to introduce the load control as a temporary measure to stabilize the system by decreasing power swings, until additional damping measures are activated. If successful, such control scheme can be effective in avoiding the current situation where the system has to be separated into two islands as the existing measures are too slow to damp power swings. The possibilities to do this have been explored here in [6].

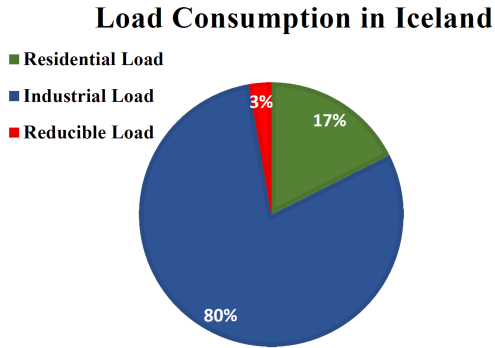


Figure 1.3: A chart of the types of load consumption in the Icelandic Power Network [9].

1.2 Objectives

1.2.1 General Objectives

The objective of this project was to develop a load control algorithm for damping inter-area oscillations and test it using the two-area four-machine Klein-Rogers-Kundur power system model. The algorithm was deployed on an external controller (NI-cRIO) and tested using Real-Time Hardware-in-the-Loop simulation including PMU measurements as input signals.

1.2.2 Specific Objectives

- Develop a load control algorithm to damp inter-area oscillations.
- Deploy the algorithm in MATLAB/SIMULINK, for simulation purposes.
- Test the implementation using RT-SIL (Real-Time Software-in-the-Loop) with the two-area four-machine Klein-Rogers-Kundur power system model to validate the load control algorithm design.
- Implement the algorithm on the NI-cRIO platform. Test the implementation in RT-HIL (Real-Time Hardware-in-the-Loop), and use PMU measurements as an input.
- Perform a comparative assessment between RT-SIL and RT-HIL results.
- Adapt the load control algorithm with different local and remote synchrophasor measurements.

1.2.3 Assumptions and Limitations of the Project

Several choices have been made to limit the scope of the project. The list is given below.

- The study was limited to consider only one inter-area oscillation. The Icelandic system, and most other power systems, have several modes that need to be considered.
- The tests were carried out using the two-area four-machine Klein-Rogers-Kundur power system model. This model resembles the Icelandic network with two main areas and a unidirectional flow from one area to the other, it also depicts a single inter-area mode of oscillation.
- The aluminium smelters (loads) were not modelled in detail. Aluminium smelters are represented using three phase dynamic loads. This assumption is valid only as a first step to evaluate the potential of load control, but may be insufficient for performance and stability analysis.
- It was assumed that the load could be increased and decreased instantaneously. Aluminium smelters load demand can be increased instantaneously, however, their power output needs to be modulated within equipment constraints.

1.3. THESIS OUTLINE

1.3 Thesis Outline

The remainder of this thesis is divided into chapters as follows:

- **Chapter 2:** In this chapter, the background information needed to understand the thesis work, is presented. The phenomena of power system oscillations is introduced and methods for oscillation damping are presented. Finally, some additional information on the equipment and software used is introduced.
- **Chapter 3:** The power system simulation model used is presented together with the two load control algorithms developed. The testing approach and the testing preparations made are also introduced in this chapter.
- **Chapter 4:** In this chapter, testing results for RT-SIL and RT-HIL simulations are shown and analysed.
- **Chapter 5:** Conclusions about the work are drawn and future work and recommendations are discussed.

Chapter 2

Background

2.1 Power System Oscillations

Inter-area power system oscillations have been observable in electric power systems ever since groups of isolated synchronous generators have been interconnected to neighbouring networks. These oscillations typically occur between groups of generators connected through weaker power transfer corridors. In steady-state, the input mechanical torque and the output electrical torque remain constant for each machine in the system. A small load change in the system can upset the balance and result in a mismatch between electrical and mechanical torque. In general oscillations can be initiated by random and small load changes, and are acceptable if they are damped quickly. An example of good damping of oscillations in the Icelandic power system captured from real PMU measurements are shown in Fig. 2.1. A fault occurs at $t = 590$ s, when an industrial load is disconnected without notice. This results in a damped angular difference between the substations of $\approx 8^\circ$ which are subsequently damped in ≈ 10 s by the controls in the system. However, observe that the random load variations cause a large angle difference deviation at $t = [600 - 630]$ as compared with $t = [530 - 590]$.

The nature of these oscillations is determined by the system's characteristics. Each power system contains a set of electromechanical modes, varying with changes in system topology. These modes can either be local or inter-area. When an oscillatory mode involves only a small part of the system it is called a local mode. They can be oscillations of a single generator or a plant against the rest of the system or oscillations between a few generators that are located close together and are commonly in the frequency range 0.8 – 2 Hz. Inter-area modes on the other hand, involve a wide-spread part of the system. These modes involve oscillations between a group of generators in one area swinging against a group of generators in another area and are most common in the frequency range 0.1 – 1 Hz [3].

In the Icelandic network there are several observable local and inter-area oscillatory modes [1]. Two inter-area modes exist, a 0.6 Hz mode that is dominant in the north-east part of the island and a 0.8 Hz mode with the same participants as

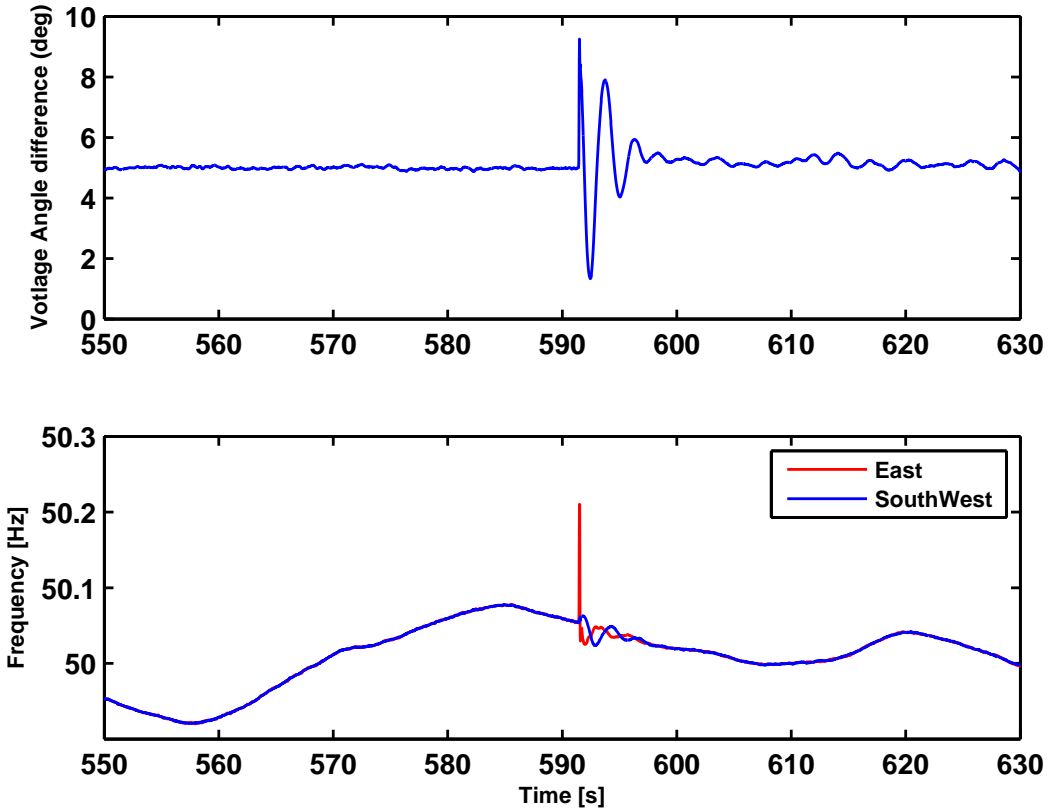


Figure 2.1: Oscillations in the Icelandic power system that are damped.

in the 0.6 Hz mode.

The Icelandic power system has large industrial loads as mentioned in Section 1.1. Industrial loads, in particular aluminium smelters, are very sensitive to change in the voltage and frequency of the grids and are prone to tripping when there is a disturbance in the grid. When this happens, for example in the south-western part of the system, the generators begin to accelerate, however, the generators closer to the load loss accelerate faster than the remote generators, leading to rotor angle separation, and loss of synchronism. This results in inter-area oscillations that can cause the transmission limit in the weak tie-line between the two areas to be exceeded and the system has to be islanded. In Fig. 2.2 the growing oscillations caused by an critical line being tripped in the south-western corner is shown. It finally results in the islanding of the system at time $t = 590\text{s}$. Voltage angle difference measurements are used because it gives a good overview of how the system falls out of synchronism and is finally islanded. These measurements can be used to identify the inter-area oscillation cases that result in islanding the system and to trigger control actions.

2.2. POWER SYSTEM OSCILLATION DAMPING

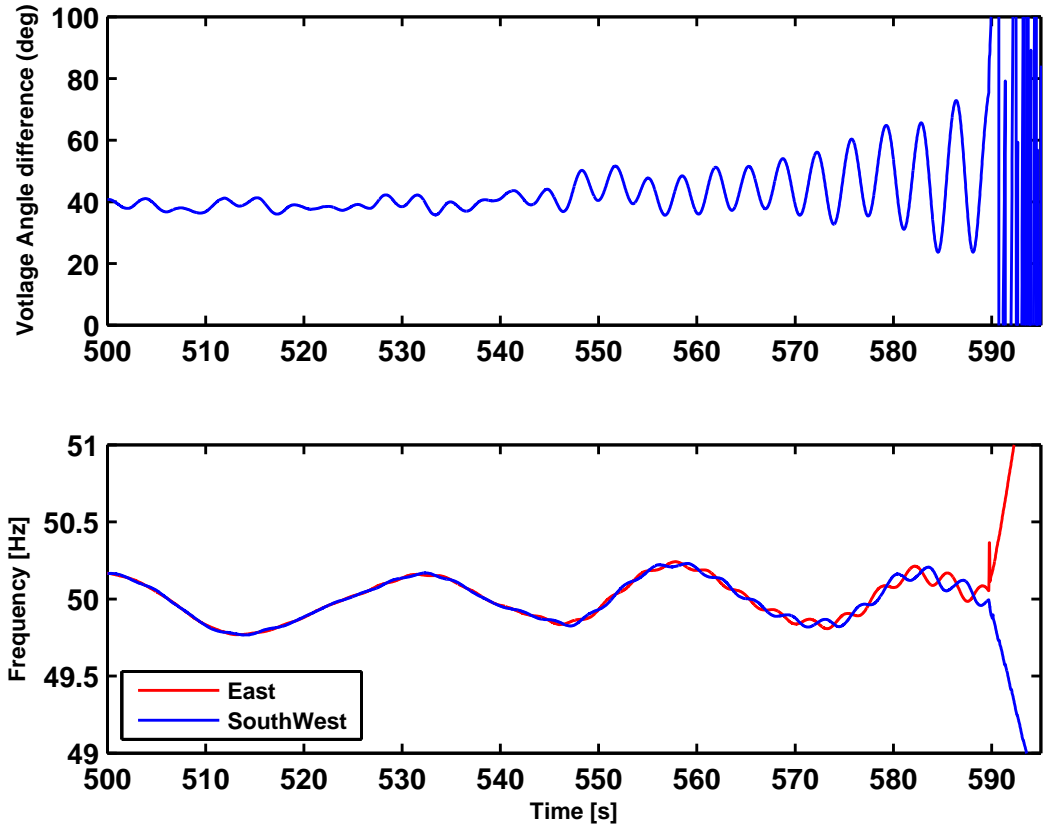


Figure 2.2: Inter-area oscillations in the Icelandic power network that increase until the system is islanded.

2.2 Power System Oscillation Damping

2.2.1 Means for damping of inter-area oscillations

In order to damp power oscillations and avoid system islanding, additional devices need to be installed in the power system. Traditionally power systems have relied on Power System Stabilizers (PSS), a part of generator control equipment, for damping of power oscillations. It provides a supplementary input signal to the excitation system of the synchronous generator for oscillation damping [11]. In latter years, supplementary control of Flexible AC Transmission System (FACTS) devices became a suitable option to provide additional damping of inter-area oscillations. FACTS devices are power electronics-based systems used to control one or more AC transmission quantities to enhance controllability and to increase power transfer capability of the network [12]. High-Voltage Direct Current (HVDC) transmission links may also contribute to damping of inter-area oscillations because the power flow through the link can be controlled independently of the ac systems it is interconnecting [13].

2.2.2 Conventional Control Approach

The conventional control approach for design of PSS and FACTS for damping requires a linear model of the system. This design based on linear control theory, is carried out off-line for one or several operating points in the system and has fixed parameters once deployed in the hardware. Thus, this approach only provides optimal performances for the specifications made during the design. Because of the non-linear characteristics of the system, the same level of quality can not be guaranteed when the operation conditions of the system change [11]. In many cases the control parameters have not been updated since the controller was installed even though large changes have been made to the system topology. Therefore, these types of damping controllers are not being used to their full potential.

2.2.3 Phasor-Based Control Approach

An alternative to the conventional control approach described above is the phasor-based approach. The phasor-based approach uses the fact that the frequency of the potential inter-area oscillation is typically well known. However, if not known there are many signal processing methods that can be used to determine it both off-line or on-line [14].

The phasor-based approach aims to solve the problem by separating the oscillatory content and the measured average value of the signal for that certain frequency of oscillation. The measured input signal can be represented as a space vector [15].

$$S(t) = S_{av} + Re\{\vec{S}_{ph}e^{j\omega t}\} \quad (2.1)$$

The space phasor representing the oscillatory content of the measured signal can be separated into two components, the real and the imaginary part, in a rotating d-q axis reference frame, as follows

$$S(t) = S_{av}(t) + S_d(t)\cos(\varphi(t)) - S_q(t)\sin(\varphi(t)) \quad (2.2)$$

where

$$\varphi(t) = \omega t + \varphi_0 \quad (2.3)$$

The angular frequency of the rotating d-q frame is ω and φ_0 is the phase angle that the space-phasor is locked to the reference frame at. Thereby, the average value, $S_{av}(t)$, which is slowly varying is separated from the oscillatory content, \vec{S}_{ph} . To estimate the average and the d-q components either a low pass filter (LP) or a recursive least square filter (RLS) can be used.

The advantage of using the phasor-based approach is that a model of the system is not required. It is also computationally efficient, offers phase correction and can damp multiple oscillatory modes. The limitations are that the algorithm takes one swing to lock itself to the set frequency and its performance can be highly non-linear and complex.

2.3. WIDE-AREA MONITORING AND CONTROL

2.3 Wide-Area Monitoring and Control

For many years local measurements have been used as input signals for PSS controllers and FACTS devices [16]. They have been preferred over remote measurements, guaranteeing a simpler and more reliable signal acquisition system as compared to communicating measurements in real-time over long distances. Available local measurements may, however, have a too low observability, thus preventing efficient control of the oscillations.

Technological progress in computer and communication technology makes it now possible to consider remote measurements. Using wide-area controllers has shown potential to give better observability of inter-area oscillations [17], provide more choices for control signal and to make it easier to use measures of controllability and observability to find the optimal input and output signals [18].

The use of wide-area measurements for damping control has been a popular topic in research for several years but only a few implementations have been built and tested. In China, a WADC (Wide-Area Damping Control) was used to modulate the output of two HVDC lines. This was the first time PMU measurements were used as an input signal for a continuous feedback control system [19]. In Norway, a WAPOD control for SVC has been successfully implemented [12]. In Section 1.1 and further in [6], the use of wide-area measurements in the Icelandic network for monitoring, defence and control are listed.

2.3.1 Phasors and Synchrophasors

A sinusoidal waveform can be represented in the time domain as shown in equation (2.4)

$$X(t) = X_m \cos(\omega t + \phi) \quad (2.4)$$

where X_m is the magnitude of the waveform, ω is the angular speed and ϕ is the angular starting point for the waveform. When analyzing AC signals in power systems with constant frequency the signals are often represented using phasors as shown in equation (2.5)

$$X = \frac{X_m}{\sqrt{2}} e^{j\phi} \quad (2.5)$$

The phasor depends on the RMS value, $X_m/\sqrt{2}$, and the phase angle ϕ that is relative to a certain reference. Phasors are defined for a certain angular speed ω . It has to be taken into account that phasors are defined for different angular speeds, i.e. system frequency [20], in Europe 50 Hz and in North America 60 Hz.

A synchrophasor is defined as the magnitude, $X_m/\sqrt{2}$ and angle ϕ of a cosine signal in reference to a cosine function at nominal system frequency that is synchronized to Coordinated Universal Time (UTC) as shown in Fig. 2.3. This allows the magnitude and the phase of the signal to be referred to the same reference for the three different phases. Usually synchrophasors are presented as angles between -180° and 180° rather than 0° to 360° [21].

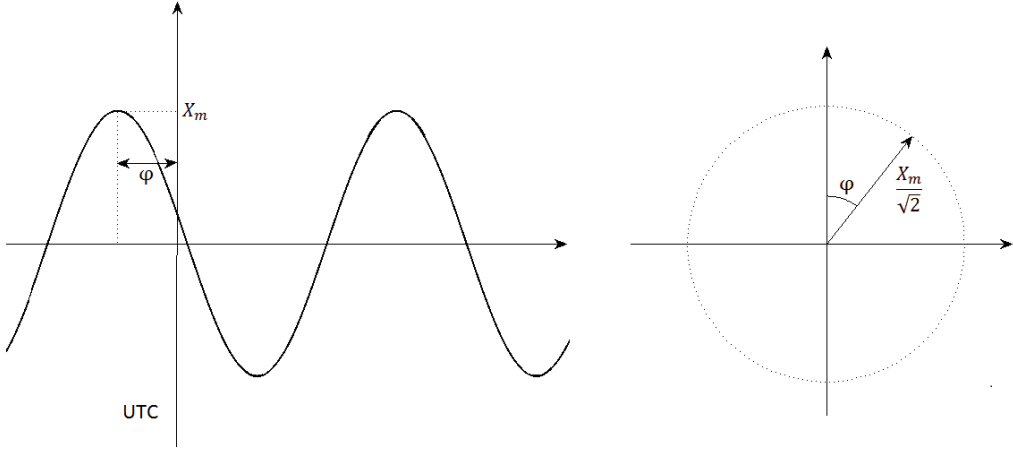


Figure 2.3: The relation between a phasor measurement and a sinusoidal waveform.

2.3.2 PMUs and PDCs

A Phasor Measurement Unit (PMU) is a device that computes synchrophasors, system frequency estimates, Rate-of-Change-of-Frequency (ROCOF), etc. The analog inputs of a PMU are current and voltage measurements taken from the secondary windings of current and voltage transformers for all three phases. PMUs are equipped with GPS receivers which enables time-stamping and time-syncing of measurements from different parts of the system [20]. It allows the system operator to have a time-stamped snapshot of the power system behavior. The time accuracy of the GPS should be $1\ \mu\text{s}$ which corresponds to 0.018° for a 50 Hz system [21]. The PMU architecture is shown in Fig. 2.4.

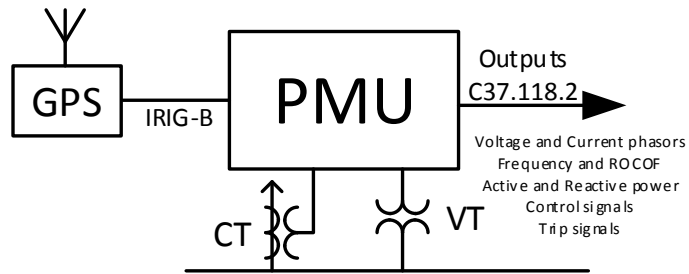


Figure 2.4: Overall architecture of a PMU.

2.3. WIDE-AREA MONITORING AND CONTROL

The measurements from several PMUs are gathered and time synchronized in a Phasor Data Concentrator (PDC). The PDC can be used for both gathering data from numerous PMUs and/or PDCs and for creating a system-wide measurement set. Each substation can have several PMUs and a PDC to collect the measurements and forward them to an upper layer PDC. There can be many layers of PDCs for different levels of the system but, finally, all the data is collected in a PDC that is often located at a control center and is often termed as "Super PDC". At every level the measurements can be monitored, stored or used for control [22]. A basic structure of a synchrophasor data network is shown in Fig. 2.5

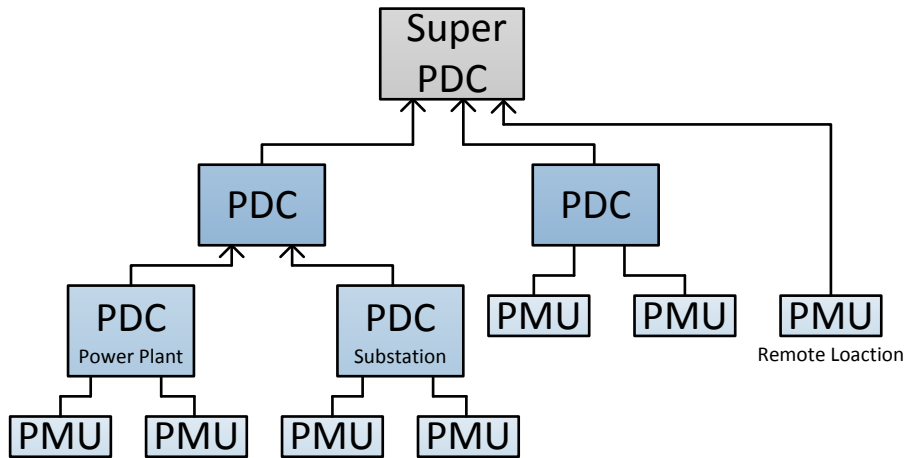


Figure 2.5: An example of a basic structure of a synchrophasor data network.

The IEEE C37.118 standard provides a protocol for the frame of messages sent from PMU/PDC. The C37.118.2 message protocol defines the following four frame components[20]:

- **Data Frame** contains the measurements from a PMU, sent from the PMU/PDC.
- **Configuration Frame** contains a machine-readable message that describes the data types, calibration factors and other information on the data being sent from the PMU/PDC.
- **Header Frame** consists of a human readable descriptive information provided by the user and sent from the PMU/PDC.
- **Command Frame** consists of machine-readable codes sent to the PMU/PDC for control or configuration.

2.3.3 Laboratory Infrastructure for Implementing and Testing

The motivation behind setting up the Smart Transmission System Laboratory (SmarTS Lab) at KTH was to develop different wide-area monitoring, protection and control (WAMPAC) applications, that exploit PMU data and can thereby make the operation of power systems safer, more efficient and more reliable. The setup includes a Phasor Data Concentrator (PDC) that uses the software solutions from Schweitzer Engineering Laboratories (SEL). The devices connected to the PDC are commercial PMUs from SEL, ABB and Arbiter and a custom NI-cRIO PMUs. Figure 2.6 shows the architecture of the SmarTS Lab [23]. In the lab, both Real-Time Software-in-the-Loop (RT-SIL) and Real-Time Hardware-in-the-Loop (RT-HIL) experiments can be performed.

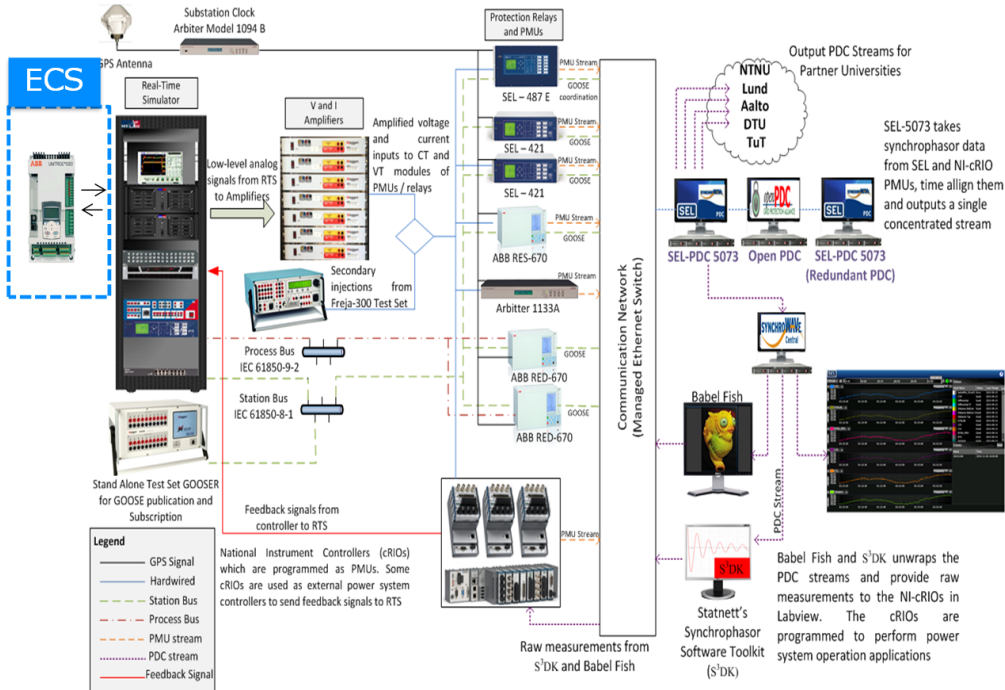


Figure 2.6: The SmarTS Lab setup.

eMEGASIM Real-Time Digital Simulator and MATLAB/Simulink

For performing real-time simulations, a eMEGASIM Real-time digital simulator from OPAL RT is used [24]. It has two targets, each running on 12-core 3.3 GHz Inter i7 processors. Models developed in MATLAB/SIMULINK can be simulated in real-time using this platform.

SIMULINK is a graphical programming environment for multi-domain simulation. It is different from other conventional programming languages. Instead of writing

2.3. WIDE-AREA MONITORING AND CONTROL

code, blocks and wires are connected together. It comes with a customizable set of block libraries and has various extension toolboxes. SIMULINK was developed by MathWorks and is integrated extensively with the rest of the MATLAB environment [25]. In this thesis, the SIMULINK extension SimPowerSystems toolbox has been used. SimPowerSystems allows the user to rapidly and easily build and simulate power system models [26]. RT-Lab which is the development environment for the eMEGASIM simulator only uses MATLAB/SIMULINK as a graphical programming interface. To be executed on the simulator the models are compiled into C-code.

Interactions between the simulations on the eMEGASIM simulator and external devices can be done either through the simulator's low-power analogue outputs and inputs or with data streamed over TCP/IP, UDP, etc. The Analog Outputs and Inputs for the simulator are listed here below.

- Analog Output: 32($\pm 10\text{ mA}$ and $\pm 16\text{ V}$)
- Analog Inputs: 128 ($\pm 10\text{ mA}$ and $\pm 100\text{ V}$)

This is not a complete description of features of the simulator but the information given here is relevant to this thesis. For a more detailed description of the simulator's capabilities and more information on the SmarTS Lab, see [27].

LabVIEW and NI-cRIO

LabVIEW, similar to MATLAB/SIMULINK, is a graphical programming platform developed by National Instruments. It can be used for system design, development and testing [28]. Various versions and extensions are available for LabVIEW but in this thesis the LabVIEW Real-Time Module and the LabVIEW FPGA modules are used. The Real-Time module combines real-time operating systems with the graphical programming of LabVIEW allowing to build real-time applications [29]. The LabVIEW FPGA Module compiles LabVIEW code to FPGA hardware [30].

The NI-Compact-Reconfigurable-I/O (NI-cRIO) is a modular, reconfigurable control and acquisition system that can be programmed using the LabVIEW FPGA module and Real-Time module. It is designed for development of embedded control and monitoring applications. It consists of an embedded controller for communication and processing in real-time, a reconfigurable FPGA chassis and swappable I/O modules [31].

Chapter 3

Load Control Algorithm: Design and Testing

3.1 The Test Power System Model

The aim of the thesis was to develop a load control algorithm for damping inter-area oscillations in the Icelandic network. In order to simplify the testing procedure, the two-area four machine Klein-Rogers-Kundur power system model was chosen [32]. This model resembles the Icelandic system with its two areas interconnected through weak and heavily loaded tie-lines. The areas are identical in every way except for the loading and the inertia coefficient for the generators. The load is divided between the two areas in such a way that Area 1 is exporting about 416 MW to Area 2. The inertia coefficient for the generators in Area 1 is 6.5 s while it is 6.175 s for the generators in Area 2. The single line diagram of the power system model is shown in Fig. 3.1. This difference in inertial gives rise to inter-area oscillations between the two areas. The system is inherently unstable and if no additional oscillation damping measures are provided, the system collapses. The test power system model parameters are listed in Appendix A.

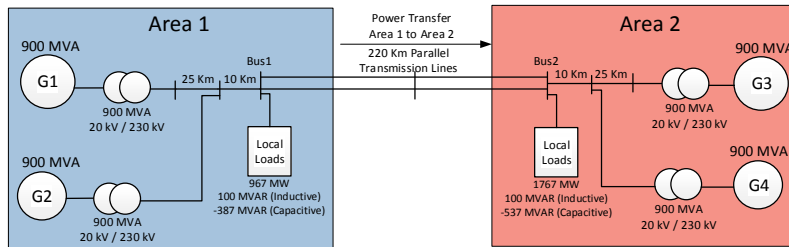


Figure 3.1: The two-area four-machines Klein-Rogers-Kundur power system model.

3.2 The Load Control Algorithm

In this chapter the load control algorithm implemented for damping of inter-area oscillations is presented. The load control algorithm is designed for damping of a certain known inter-area mode. It takes in an input signal that can be either local or remote synchrophasors measurements. The algorithm is inspired from the phasor-based power oscillation damping (Phasor POD)¹ algorithm proposed in [33] and is shown in Fig. 3.2. The algorithm has two versions with different strategies for load control. These two versions are called Algorithm 1, presented in Section 3.2.2 and Algorithm 2, presented in Section 3.2.3.

3.2.1 Phasor POD

The Phasor POD algorithm can be used to separate the input signal into two parts, its average value and its oscillatory content. Additional parameters are required for the algorithm, the inter-area frequency w_{cs1} , the sampling time T_s and the phase correction (α). First a ramp integrator is used taking w_{cs1} and T_s as inputs which is then followed by a Recursive Least Squares based Phasor Estimator. Finally a function block is used on the oscillatory content to implement a co-ordinate transformation. In steady-state, the extracted oscillatory content phasor is zero, but when power oscillations occur subsequent to faults or disturbances, it amplifies the oscillations. It was originally developed in [33] for controlling a Thyristor Controlled Series Capacitor (TCSC) but is applicable for other FACTS devices and for PSS. The algorithm also facilitates phase compensation so that both local and remote synchrophasor measurements can be used in the damping algorithm.

This algorithm was selected because its settings are independent of the network topology. The only configuration needed for the algorithm is the frequency of oscillation for the mode that needs damping. This frequency is usually well known. Another reason is its flexibility with input signals allowing different local and remote synchrophasor measurements to be used as inputs without having to make any changes to the algorithm, except appropriate phase angle compensation.

3.2.2 Algorithm 1

The input to the algorithm, as shown in Fig. 3.3, is the oscillatory content that is generated by the Phasor POD algorithm. The input signal that was first used for developing the algorithm was the active power transfer from Area 1 to Area 2. In the presence of inter-area oscillations, the active power being transferred between the two inter-areas is greater than the steady-state active power transfer for half of the oscillatory frequency cycle and less than the steady-state active power transfer

¹Historically, damping stabilizers have been termed POD where the P represents a measurement of active power through the line. Active power here would be used as a controller input signal. Although this term is not accurate when other quantities are used as control inputs or feedback signals, the term is used here to maintain consistency with existing literature.

3.2. THE LOAD CONTROL ALGORITHM

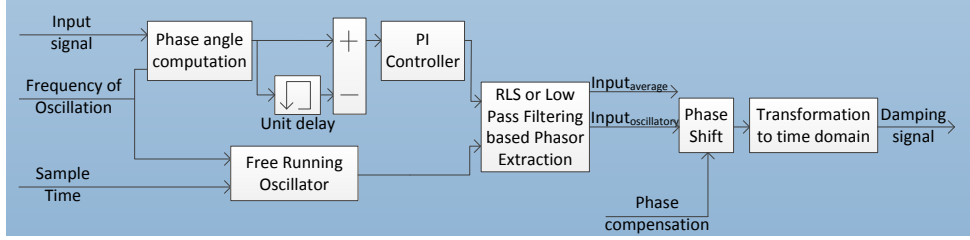


Figure 3.2: The Phasor POD algorithm.

for the other half of the cycle. The control signal for the active load modulation is created by first finding the derivative of the oscillatory part of the input signal. When the active power transferred is increasing, the load control sends a command to the load in Area 2 to increase its active power consumption. On the other hand when the power transfer is decreasing, a command is sent to the load in Area 2 to decrease its active power consumption. The amplitude of load change is determined by the maximum value of the oscillatory signal for increase in load and in the same way, the minimum value for the decrease reset for each cycle. In order to use other input signals, the phasor compensation capability the Phasor POD algorithm is exploited.

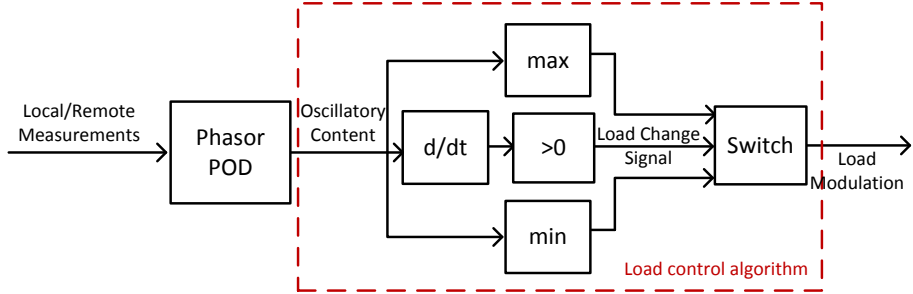


Figure 3.3: Active load control Algorithm 1.

3.2.3 Algorithm 2

The second algorithm is almost exactly the same as Algorithm 1. The algorithm increases the active load when the power transfer is increasing in the same way as before but the main change is that for decrease in active power transfer between the two areas, the algorithm is blocked so it does not allow load shedding. This is done

to give additional flexibility to the TSO to reach sufficient damping while avoiding load shedding that can be a costly measure [34].

3.3 Algorithm Testing Approach

The development process used to design the active load controller is the V-model. The V-model is a modified version of the traditional waterfall model that emphasises on verification and validation. The V-model used can be seen in Fig. 3.4. The process starts in the upper left and goes to the upper right. In the left leg of the V, the design and software development takes place, and in the right leg, HIL testing is performed on the developed software. Each step in the left leg has a matching testing step on the right leg and each phase must be completed before the next phase is started. This means that in each phase the hardware components are tested against the specifications [35]. The algorithms were tested in the four stages shown in Fig. 3.4, these stages will be explained in more detail in Chapter 4.

Observe that one particular challenge to apply the V-model in this work is that the design and development environment for the algorithm design (i.e. MATLAB/SIMULINK) is completely different from the one used for implementing and testing (i.e. LabVIEW on NI-cRIO). This implies that a complete implementation of the algorithm had to be carried out in each environment.

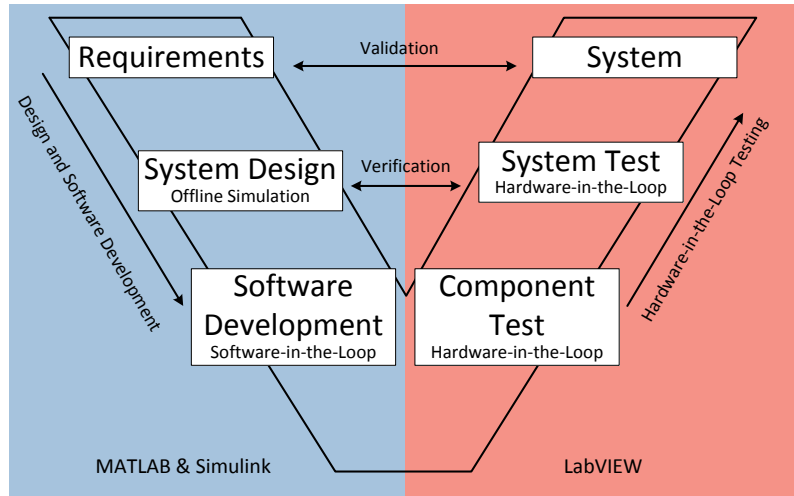


Figure 3.4: The V-model for developing the load control algorithm.

3.4 Testing Preparation

In the following section's the preparations needed for testing the algorithm are listed.

3.4. TESTING PREPARATION

3.4.1 Preparation of the Simulink Model for Offline Simulation

The Simulink model used in this thesis is built on the model created for PSS performance studies by Kamwa [36]. In this power system model, three oscillation modes are observed, two local modes and one inter-area mode. The inter-area mode results in the generators in Area 1 oscillating against the generators in Area 2 with the frequency 0.64 Hz.

The load control algorithms were modelled in Simulink, see Fig. 3.5, and were set to control the load in Area 2 since power is being exported from Area 1 to Area 2 in the power system model.

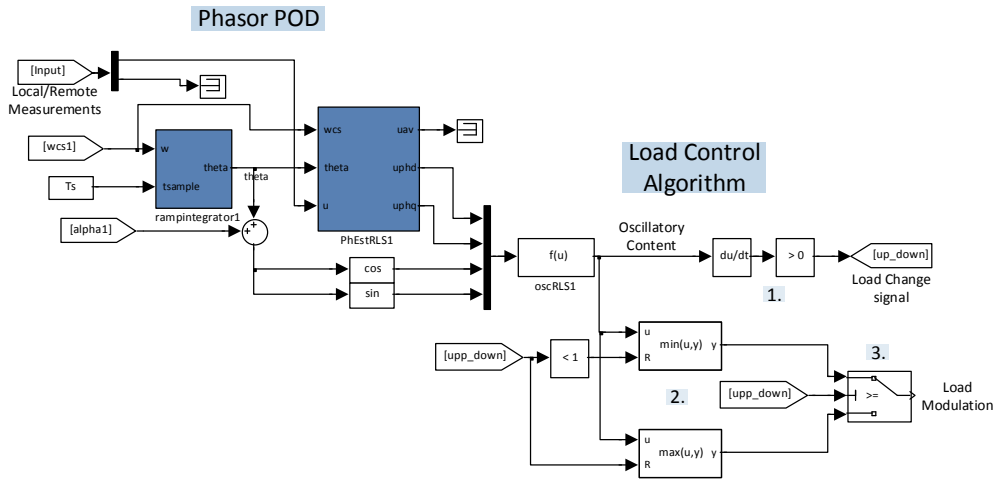


Figure 3.5: The load control implementation in Simulink.

The load control algorithm implemented in Simulink works as follows.

1. Find the derivative of the oscillatory content to determine where the oscillation reaches its maximum and minimum value.
2. Check the minimum value and the maximum value of the oscillatory content at each peak, reset every cycle.
3. The load change signal (up_down signal) determines whether to increase and decrease the load.

3.4.2 Modifications for Real-Time Simulation

To execute the Simulink model on the eMEGASIM OPAL-RT simulator, several modifications have to be incorporated. Firstly, the model has to be separated into subsystems, each of which will be executed on a separate core. There are three types of subsystems available. Every model needs to have a *Master Subsystem* that

CHAPTER 3. LOAD CONTROL ALGORITHM: DESIGN AND TESTING

is responsible for the model's real-time calculations, I/O communication and the overall synchronization of the network. *Slave Subsystems* can be used in the model for additional computation elements. Each model can only have one Master Subsystem but it can have several Slave Subsystems. The third type of subsystem is the *Console Subsystem* that contains the part of the model where the user can interact with the running model and monitor the model parameters. Only one Console Subsystem can be used per model. Each subsystem is allocated on one process core in the real-time simulator. Simple feed-through blocks called OpComm must be added to the model to ensure synchronisation of the subsystems. They intercept all incoming signals before sending them to computation blocks in the given subsystem [37].

The two-area system was grouped into the following subsystems. The Master Subsystem included all the elements of Area 1. Two Slave Subsystems were used, the first one contained Area 2 and the second one included measuring and monitoring of line parameters as well as the load control algorithm for Software-in-the-Loop and communication with the load control algorithm for Hardware-in-the-Loop. A Console Subsystem was used for monitoring and control during simulation. This can be seen in Fig. 3.6.

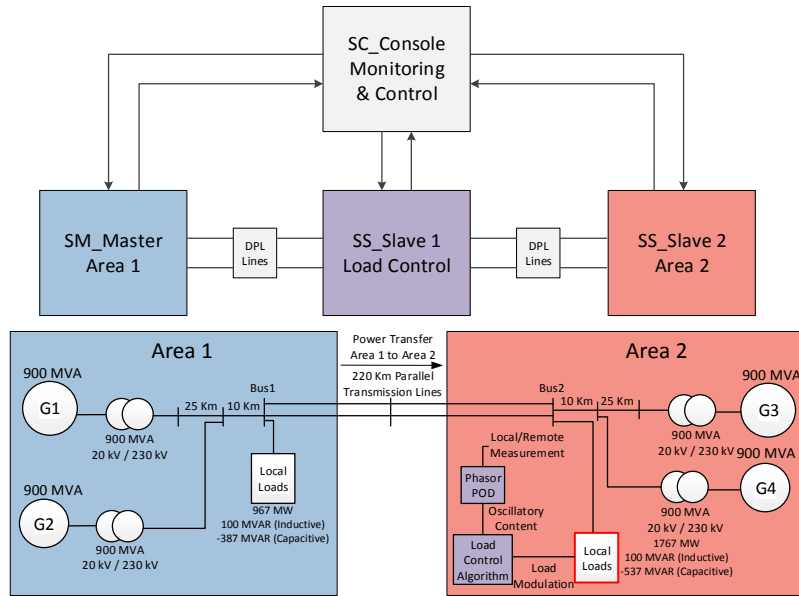


Figure 3.6: Shows how the two-area power system model and the load control algorithm is devided into subsystems.

The steps followed for RT-SIL validation are shown in Fig. 3.7. The power system model and the load control are simulated on two separate cores on the simulator. The control signal from the load control algorithm is fed to one of the digital

3.4. TESTING PREPARATION

outputs of the simulator and then looped back through one of the inputs of the simulator. The feedback signal received through the digital input then modulates the active load consumption of the dynamic load in Area 2. The model was executed in real-time with a step size of $50\ \mu s$.

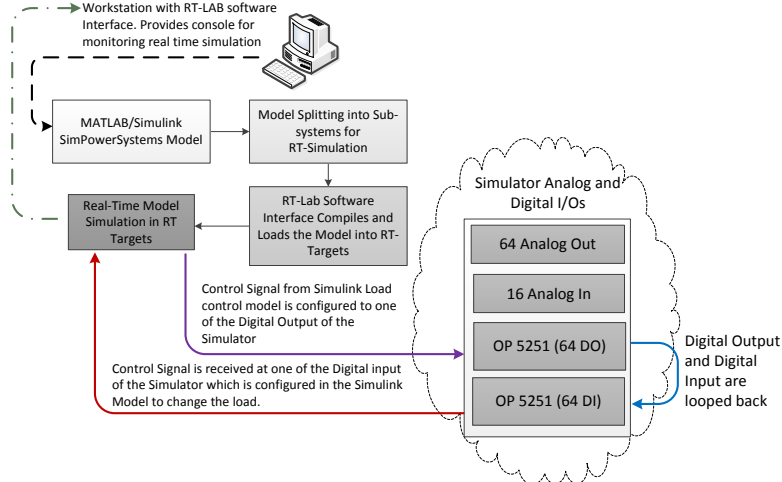


Figure 3.7: Steps for RT-SIL simulation.

3.4.3 Hardware-in-the-Loop Execution

To perform the RT-HIL simulations in SmarTS Lab the setup shown in Fig. 3.8 is used. Each step in the setup is listed below and, in the following sections, explained in more detail.

1. Execute the two-area four-machines Klein-Roger-Kundur power system model in the real-time simulator.
2. Send voltage and current signals to PMU(s).
3. The PMU(s) compute(s) synchrophasors and forward(s) the stream(s) to the PDC for concentration and archiving.
4. S³DK [23] unwraps the PDC stream and gives raw measurements (phasors, analogs and digitals), in the LabVIEW environment for processing and forwarding to the load controller.
5. The load control algorithm deployed in the NI-cRIO (FPGA).
6. The Load modulation signal is sent back to the Real-Time simulator.

CHAPTER 3. LOAD CONTROL ALGORITHM: DESIGN AND TESTING

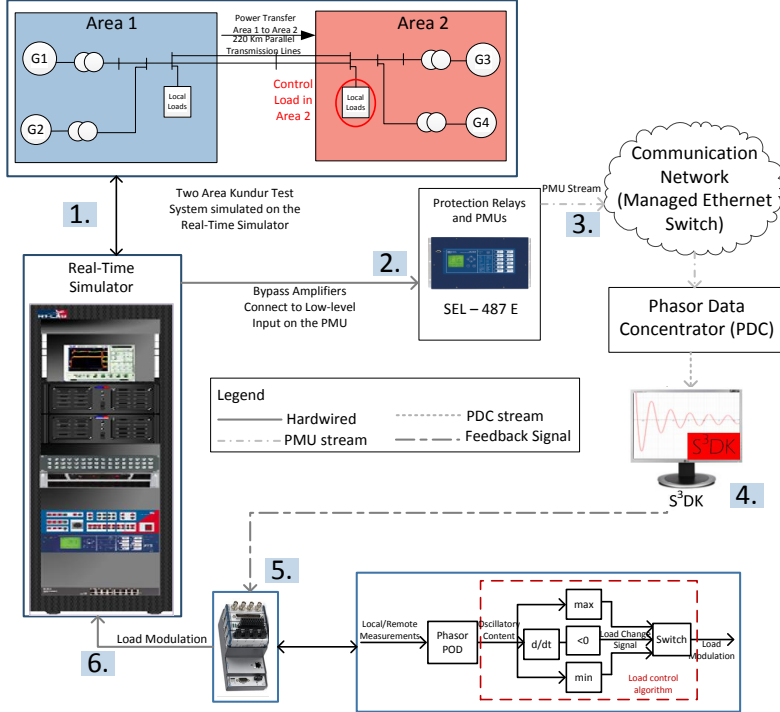


Figure 3.8: Shows the RT-HIL setup used.

Real-Time Simulation Model Preparation

To communicate with the external device, two types of blocks have to be added to the real-time model simulated on the OPAL-RT simulator. An Analog-In (AI) and an Analog-Out (AO) block, see Fig. 3.9 [37]. In these blocks, the AI/O used is picked as well as the number of I/O channels needed. In the power system model, voltage and current measurements were gathered in both areas of the system and sent out using an AO block. A feedback signal is then received from the external controller using an AI block. Before sending and receiving the voltage and current signals, they have to be scaled down since the simulator has limitations for the I/Os as listed in Section 2.3.3.

The PMU and PDC Connections

The SEL-421 Relay is a line distance protection, automation and control device. It can be configured to work as a PMU when combined with a GPS receiver and is used in this thesis as such [38]. As was mentioned in Section 2.3.3 the SmarTS Lab has amplifiers to step up the low level analog signals from the real-time simulator to appropriate levels for the protection relays and the PMUs. These are single phase amplifiers and therefore result in slight off-sets where amplifying the three phases.

3.4. TESTING PREPARATION

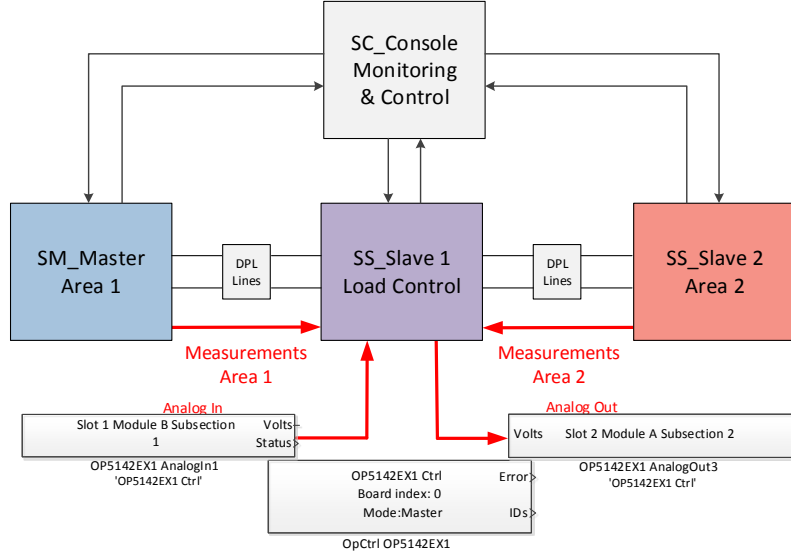


Figure 3.9: Shows where the I/O blocks are added in real-time model.

In addition, these amplifiers may cause additional time delays and because the load control has to work as fast as possible, the amplifiers are bypassed and the low-level interface of the SEL PMU is used.

Given that measurements from two remote parts of the system are being used, in reality two different PMUs should be used, one for each area. Because of limited resources only one PMU is used for the measurements from both areas since SEL-421 offers two 3-phase current channels and two 3-phase voltage channels. This simplifies the testing process because all PMUs have some inherent differences even when they are the same model from the same vendor. Because the same PMU is used, there is no need to forward the measurements to the PDC to be time aligned. In this setup, the PDC is used to try to replicate the real scenario more closely and to archive the measurements for off-line analysis. Note that in future tests more than one PMU might be necessary. The PDC then forwards the measurements to the another computer.

Deploying the Load Control on an Embedded Hardware Platform

The external controller, that the load control algorithms are deployed on, is a NI-cRIO, introduced in Section 2.3.3. The NI-cRIO that was chosen for this work is NI-cRIO-9076. It has a 4-slot Xilinx Spartan-6LX45 FPGA and is a 400 MHz processor [39].

The main aim of using this hardware platform is to develop a hardware prototype controller that is tested and validated in the SmarTS Lab environment. This controller should then be integrated in the Icelandic system to control the load with-

CHAPTER 3. LOAD CONTROL ALGORITHM: DESIGN AND TESTING

out major modifications. Therefore in the design of the controller, it is desirable that it can receive the PDC stream directly in the NI-cRIO. This is not possible since no PMU data-mediation software available today can be executed on the NI-cRIO. Instead a remote workstation is used to receive the PDC stream, which is IEEE C37.118.2 compliant. Statnett's Synchrophasor Software Development Kit (S^3DK) is used to receive and unwrap the PDC stream into raw measurements in the LabVIEW environment [23].

A three level design was chosen to implement the load control algorithm. In Fig. 3.10 the different layers in the three-level LabVIEW program that is used are shown. Indicated in red is the VI running on the external workstation, in blue is the VI running on the real-time processor on the NI-cRIO and in green is the VI deployed on the FPGA.

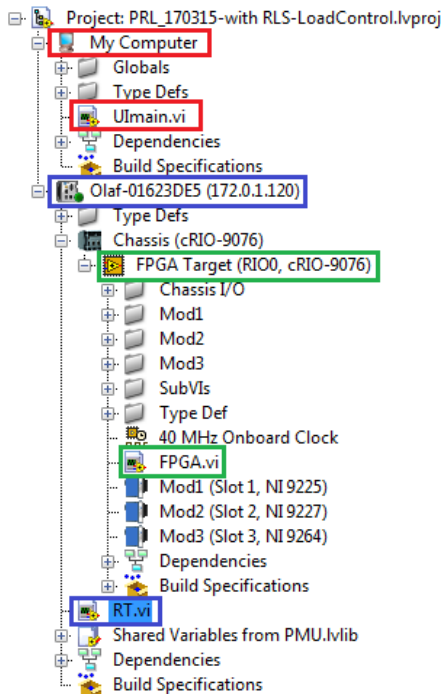


Figure 3.10: The three-level structure of the LabVIEW program used.

The three levels are explained below.

- **Remotely run VI (UImain.vi):** Runs on a typical computer. S^3DK is used to unwrap the PDC stream and then forward raw measurements to the real-time processor on the NI-cRIO.
- **Real-Time Software (RT.vi):** Runs on the real-time processor of the NI-cRIO. It handles all communication between the user and the FPGA. It receives the PMU measurements from UImain.vi and manages the signal selection and forwards the selected input signal to the FPGA.

3.5. ALGORITHM REFINEMENT

- **Core FPGA Software (FPGA.vi):** It consists of the load control algorithm that runs on the FPGA and sends out the load control signal to the AO. The loop rate of the FPGA that is used is $100 \mu\text{s}$ to avoid overruns.

The load control algorithm developed had to be replicated in LabVIEW FPGA since the algorithm was deployed on a NI-cRIO, see Fig. 3.11. The LabVIEW FPGA implementation followed the Simulink implementation as closely as possible. Some obvious differences can though be noted. In LabVIEW FPGA there is no block to find the derivative of the oscillatory part of the input signal. Instead a numerical derivative of 1st order is implemented as follows

$$\frac{\Delta x}{\Delta t} = \frac{x_2 - x_1}{t_2 - t_1} \quad (3.1)$$

where x_2 and x_1 are successive measurements of the input signal received in NI-cRIO at time t_2 and t_1 respectively. The FPGA has a fixed time step so the denominator in equation (3.1) is a constant. Therefore the derivative calculation is simplified to the numerator, that is finding the difference between the last two signals.

The three steps in the algorithm modelled in Simulink, explained in Section 3.4.1 are the same for the algorithm modelled in LabVIEW FPGA.

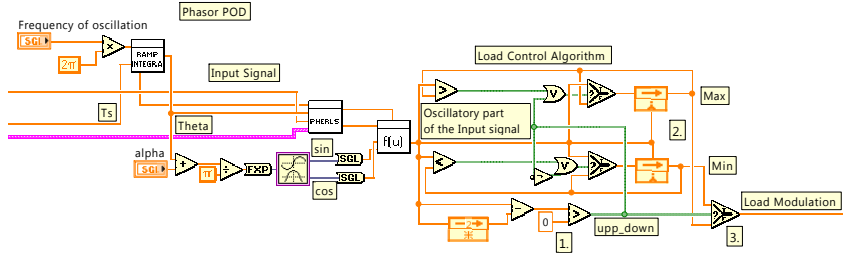


Figure 3.11: The load control algorithm implemented in LabVIEW FPGA.

3.5 Algorithm Refinement

When the algorithm was tested in RT-SIL, an unexpected behaviour was detected. In Fig. 3.12 the active power transfer from Area 1 to Area 2 is shown. A disturbance has occurred in the power system model, giving rise to inter-area oscillations. Algorithm 1 and 2 are applied to damp these oscillations. The sudden change in load due to the load control algorithms results in small oscillations in the input signal, that can be observed in the zoom in of the figure. The load control algorithm should not respond to these deviations only the inter-area oscillation that need to be damped.

Therefore an extension of the algorithm was designed. The basic idea behind this extension is to block the load change for a certain time after it has detected a

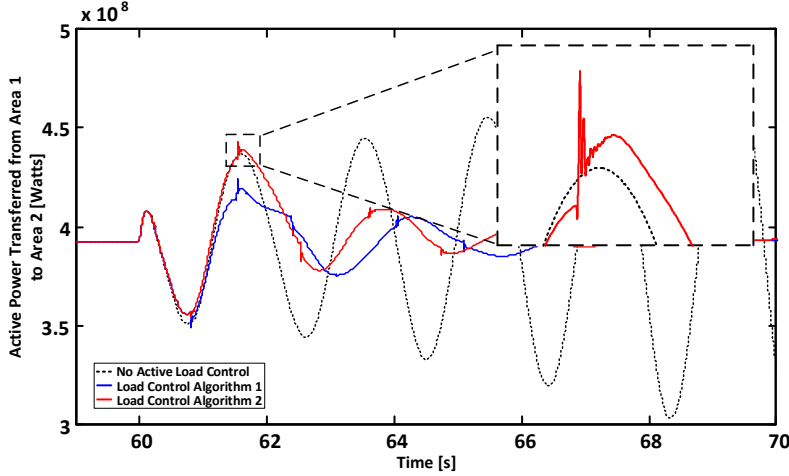


Figure 3.12: Small oscillations caused by the load control algorithm.

crest or a trough because it should stay constant until another change is detected. A counter is implemented making sure that the time between changes in the load change signal created by the algorithm is always at least equal to a pre-specified threshold. The implementation of the extension in Simulink can be seen in Fig. 3.13. Below each step of the extended algorithm is explained.

1. Take in the oscillatory content and find the derivative and the point of change (same as in the original load control algorithms).
2. Detect change in the load change signal. That is when the input to that block changes from zero to one or vice-versa.
3. A counter is implemented, which increases the count by one each cycle.
4. When the counter reaches a certain limit (here 5000 cycles) and a crest or a trough is detected, a reset signal is sent out.
5. The reset signal resets the counter.
6. The reset signal resets the load change signal (up_ down signal)

It is not enough to keep the load change signal stable, the minimum and the maximum values for the load control signal have to be kept stable for the same time period as well. Therefore, a sample and hold block is added after the block calculating the maximum and the minimum value. It can be reset by the load change signal to keep the value constant over a period of the inter-area oscillation. The implementation of this can be seen in Fig. 3.14.

The same extension was implemented in LabVIEW, as can be seen in Fig. 3.15. It has the same steps as the Simulink code, listed here above.

3.5. ALGORITHM REFINEMENT

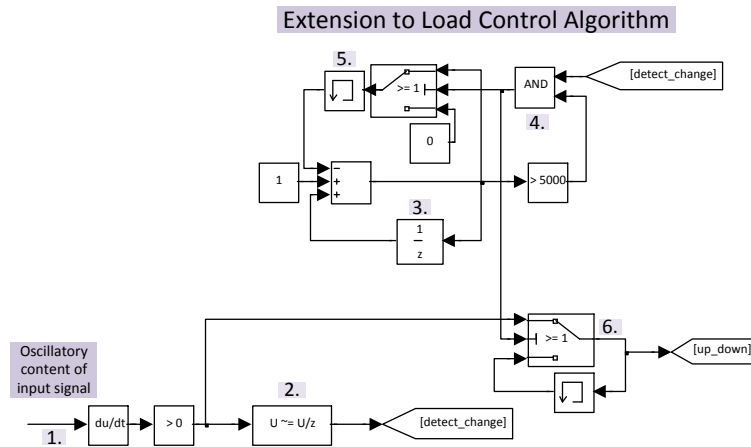


Figure 3.13: The extension added to the load control algorithm in Simulink.

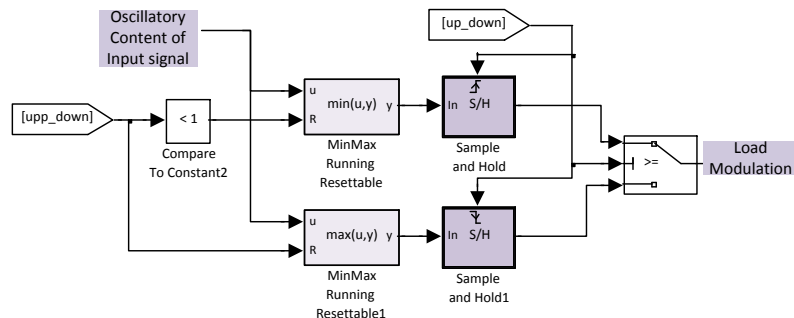


Figure 3.14: Sample and hold blocks added to the algorithm in Simulink to keep the maximum and minimum values stable.

CHAPTER 3. LOAD CONTROL ALGORITHM: DESIGN AND TESTING

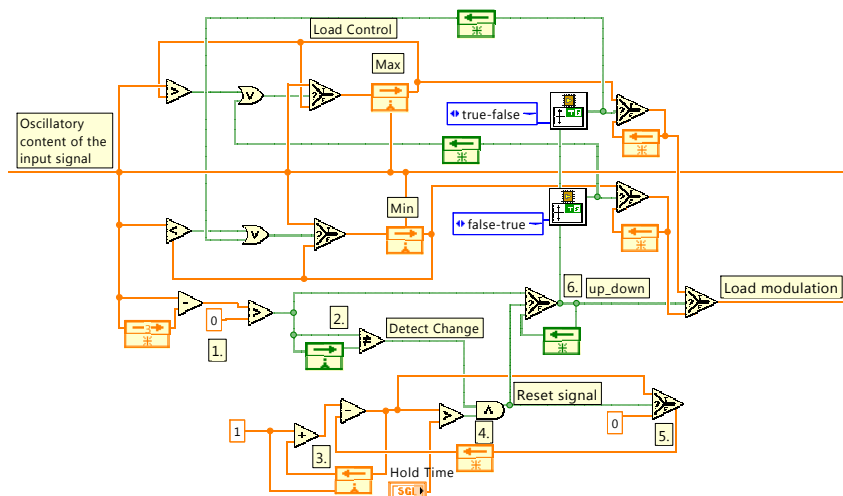


Figure 3.15: The extension added to the load control algorithm in LabVIEW.

Chapter 4

Tests and Results

The load control algorithms were tested in the following four steps that were shown in Fig. 3.4 in Section 3.3.

1. **Offline Simulation (System Design):** The two-area power system model is simulated with the load control algorithm in MATLAB/SIMULINK on the workstation computer. This is done to calibrate the algorithm and verify its functioning.
2. **RT-Software-In-the-Loop (RT-SIL) (Software Development):** The two-area power system model and the load control algorithm are both simulated in real-time on two separate cores of the real-time simulator that only communicate through signals. This is a preparation for RT-HIL to estimate the hardware resource requirements for the designed algorithms.
3. **RT-Hardware-In-the-Loop (RT-HIL) without PMU (Component Test):** The two-area power system model is executed on the real-time simulator and sends the input signal for the load control straight to the external controller through analog connections. This is done as a middle step before using the PMUs in order to foresee the modifications needed to be made to the algorithm and the challenges which might arise when using RT-HIL.
4. **RT-Hardware-In-the-Loop (RT-HIL) with PMU (System Test):** The two-area power system model is executed on the real-time simulator and sends voltage and current measurements from each area to a PMU which forwards it to a PDC. The PDC stream is received on a PC Workstation which forwards it to the NI-cRIO where the load control is implemented. The load modulation signal is finally sent back to the real-time simulator.

Results from steps 2 and 4 will be presented in the sections that follow and the difference in results caused by the time delays when simulating in HIL are highlighted. In order to analyze the performance of developed active load control algorithms, two disturbances were introduced in the power system model:

Scenario 1 A small disturbance in the form of 5% positive magnitude step in the reference voltage of Generator 1 applied for 4 cycles at $t = 60\text{ s}$.

Scenario 2 A large disturbance in the form of three phase to ground fault (4 cycles, i.e. 80 ms) at $t = 60\text{ s}$ in the middle of one of the two 220 km transmission lines connecting together the two areas.

Both these scenarios result in an undamped 0.64 Hz inter-area oscillation. Results for Scenario 1 are shown in the following sections. Results from Scenario 2 are presented in the Appendix.

4.1 Active Power as Input Signal

The algorithms presented in Section 3.2 were developed using active power as the input. It was chosen since the desired parameter to control is active power consumption of a load. The active power value used is the active power transfer from Area 1 to Area 2, measured at the middle of the two lines between Area 1 and Area 2.

4.1.1 RT-SIL

In Fig. 4.1 the performance of both the active load control algorithms are shown when the power system model is subjected to a small disturbance (Scenario 1) and is simulated using RT-SIL. If no oscillation damping control is applied to the power system model, this disturbance results in a 0.64 Hz inter-area oscillation frequency instantaneously after the disturbance is applied at $t = 60\text{ s}$. This results in the loss of synchronism between the two areas at about $t = 75\text{ s}$ and the system collapses. Both algorithms result in damping the oscillations caused by the small disturbance. Algorithm 1 provides faster damping when compared to Algorithm 2, which was to be expected since it provides damping by both increasing and shedding the active load consumption. The active power transfer from Area 1 to Area 2 (a) and the active power consumption by the dynamic load in Area 2 (b) are shown in Fig. 4.1 [34].

4.1.2 RT-HIL

In Fig. 4.2, the results for RT-HIL simulation are shown for Algorithm 1 and 2 when the power system model is subjected to a small disturbance (Scenario 1) using active power as the input signal. Again both algorithms provide damping of the oscillations and Algorithm 1 provides quicker damping than Algorithm 2. Even though damping is achieved, it is achieved much slower than in RT-SIL. This is due to the delays, scaling issues and noise in the RT-HIL setup aspects, as well as the difference between the the implementation of the RT-SIL and the RT-HIL controllers. This will be listed and analysed in Section 4.3.

4.1. ACTIVE POWER AS INPUT SIGNAL

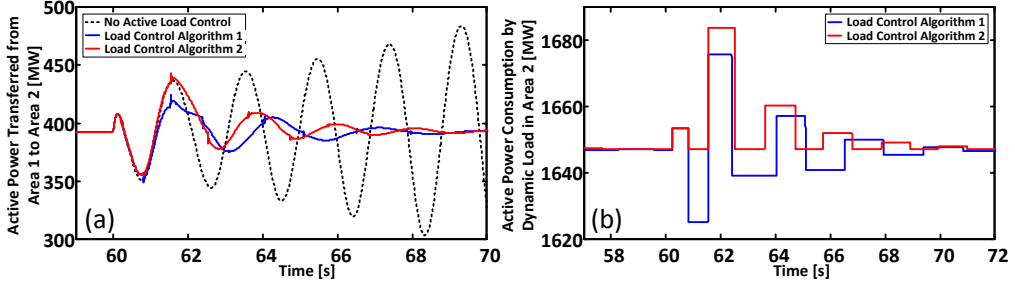


Figure 4.1: RT-SIL simulation results using active power as the input signal in the active load control algorithms.

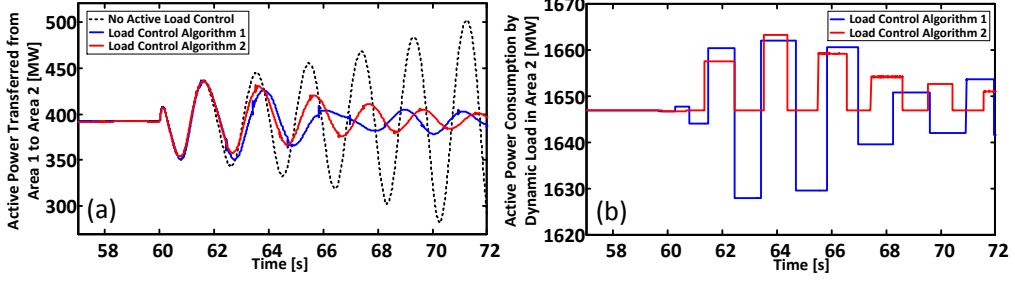


Figure 4.2: RT-HIL simulation results using active power as the input signal in the active load control algorithms.

Figure 4.3 shows the load control signal generated by the load control algorithm deployed on NI-cRIO as viewed on an oscilloscope. As can be clearly observed, the amplitude of the load change is decreasing, and thus, the oscillations are being damped. This can be viewed as further evidence that the load control signal is actually being generated in the actual NI-cRIO hardware.

4.1.3 Comparing RT-SIL and RT-HIL

Figure 4.4 shows a comparison of the RT-SIL and the RT-HIL simulation performance for Algorithm 1, with active power as input signal for Scenario 1. There it is possible to observe how much more efficiently the algorithm works in RT-SIL. There are several factors that cause this major difference between software and hardware results. These factors are for example scaling, noise and delays that the real hardware controller should expect but do not effect the SIL results.

CHAPTER 4. TESTS AND RESULTS

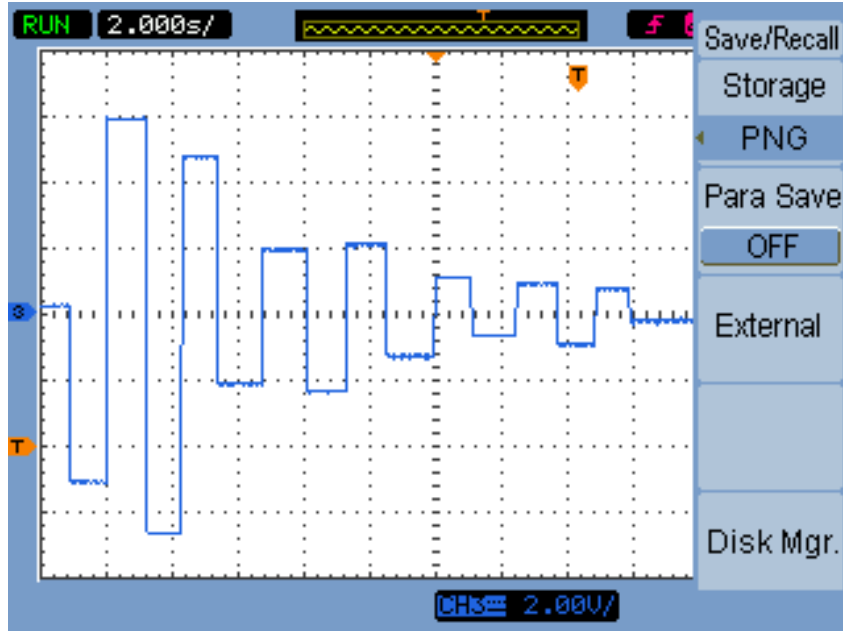


Figure 4.3: The Load control signal received from NI-cRIO seen on the oscilloscope. Active power input signal, Algorithm 1, Scenario 1. The scale is 2 V/square and 2 s/square.

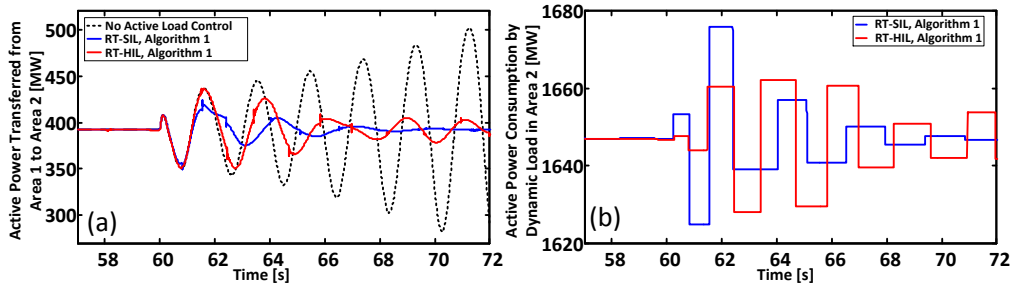


Figure 4.4: Comparing RT-SIL and RT-HIL simulation results using active power as an input singal.

4.2 Signal Selection

To find the best input signal for the load control algorithm eight different input signals were tested. The PMU locations for these different input signals are shown in Fig. 4.5. The input signals tested are listed here below.

1. Active Power transfer from Area 1 to Area 2 (P_{12}) measured by PMU located between the two areas.

4.2. SIGNAL SELECTION

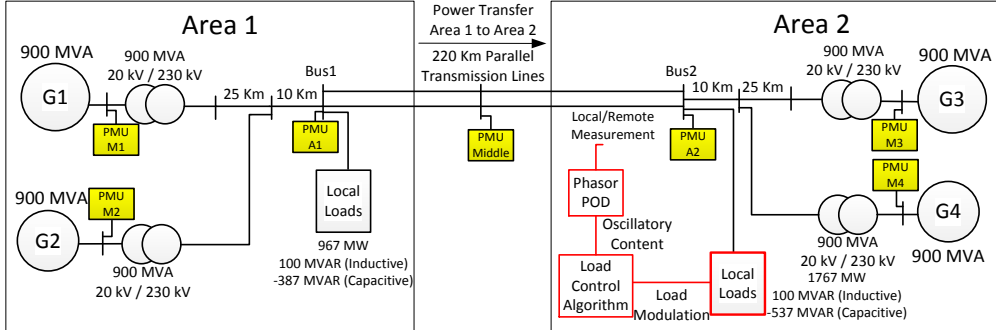


Figure 4.5: The PMU locations in the power system model.

2. Positive sequence voltage in Area 1 (V_{Area1}^+)
3. Positive sequence voltage in Area 2 (V_{Area2}^+)
4. Positive sequence current in Area 1 (I_{Area1}^+)
5. Positive sequence current in Area 2 (I_{Area2}^+)
6. The voltage phase angle difference between Area 1 and Area 2 ($V_{\varphi Area1} - V_{\varphi Area2}$)
7. The average value of the positive sequence voltage magnitude difference between Area 1 and Area 2 ($\frac{V_{M1}+V_{M2}}{2} - \frac{V_{M3}+V_{M4}}{2}$)
8. The average value of the voltage phase angle difference between Area 1 and Area 2 ($\frac{V_{\varphi M1}+V_{\varphi M2}}{2} - \frac{V_{\varphi M3}+V_{\varphi M4}}{2}$)

To test the the algorithm for the eight different input signals listed above, some adjustments were made. The phasor POD algorithm is flexible and can be adapted to any local or remote synchrophasor-based input signal without modifying the core algorithm itself. Only the phasor compensation (α) settings of the Phasor POD algorithm have to be changed depending on the input signal to compensate for the phase lag or lead between the active power transfer and the input signal. The load control signal also has to be scaled by changing the controller's gain so that the value of the load change is commensurate to the oscillations in the active power transfer. Table 4.1 shows the phase compensation and the scaling for the eight different input signals tested. Observe that the scaling factors for the signals are very big. This is because the signals have to be scaled up to MW (10^6).

4.2.1 RT-SIL

Figure 4.6 compares the results using different input signals for Algorithm 1 for Scenario 1, by performing RT-SIL simulation. There, we can clearly see that input

CHAPTER 4. TESTS AND RESULTS

Table 4.1: The phasor compensation (α) and the scaling for the different input signals of the active load control algorithms.

	Input signal	Phase Compensation α [rad]	Scaling
1.	P_{12}	0	1
2.	V_{Area1}^+	2.9125	$2.53 \cdot 10^4$
3.	V_{Area2}^+	2.9125	$2.55 \cdot 10^4$
4.	I_{Area1}^+	0	$2.3 \cdot 10^5$
5.	I_{Area2}^+	0	$2.3 \cdot 10^5$
6.	$V_{\varphi Area1} - V_{\varphi Area2}$	0	$1 \cdot 10^7$
7.	$\frac{V_{M1}+V_{M2}}{2} - \frac{V_{M3}+V_{M4}}{2}$	0	$8 \cdot 10^4$
8.	$\frac{V_{\varphi M1}+V_{\varphi M2}}{2} - \frac{V_{\varphi M3}+V_{\varphi M4}}{2}$	2.9125	$2.3 \cdot 10^7$

signal 7, the voltage magnitude difference $\left(\frac{V_{M1}+V_{M2}}{2} - \frac{V_{M3}+V_{M4}}{2}\right)$ provides the worst damping compared to the other input signals. The other input signals all achieve adequate damping in less than 10 s after the disturbance.

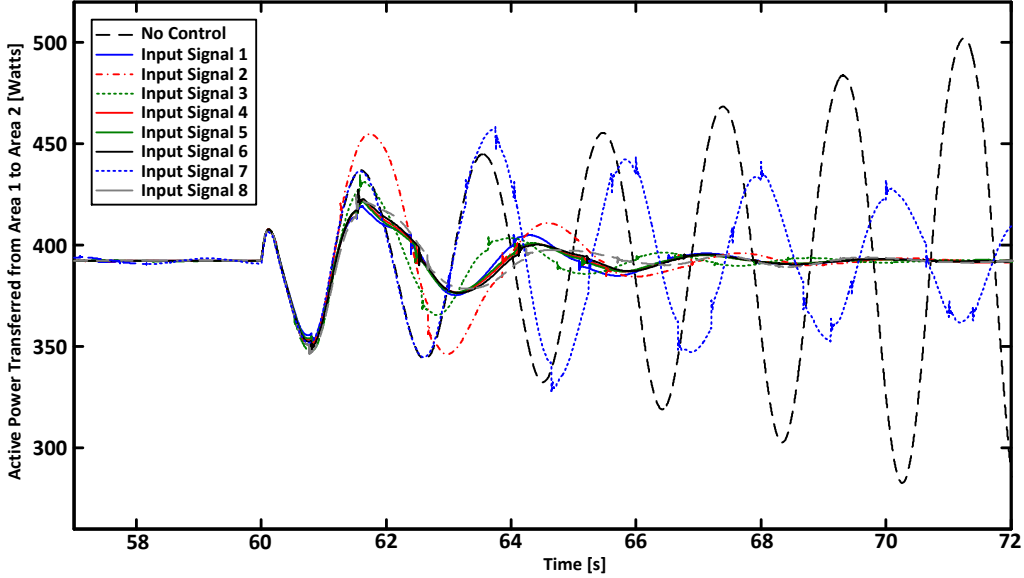


Figure 4.6: Signal selection for RT-SIL simulation using active load control Algorithm 1.

To compare the signals even further some control performance metrics are analysed. The metrics considered are *decay ratio*, *overshoot*, *undershoot* and *settling time*. Decay ratio (DR) is the ratio between the peak of the first oscillation (a) and the next peak of oscillation (b), $DR = b/a$. It shows how fast the oscillation decreases. The overshoot and undershoot are the highest and the lowest deviations

4.2. SIGNAL SELECTION

in the active power transfer after the disturbance. These are important because of the transmission limits of the line between the two areas. Finally, the settling time is calculated as the time at which the oscillations have decreased to a value that is within $\pm 1\%$ change from the original active power transfer between the areas. These results are listed in Table 4.2.

Table 4.2: Shows the four factors considered for each input signal in when RT-SIL simulation is used.

Input signal	Decay Ratio	Overshoot [MW]	Undershoot [MW]	Settling Time [s]
1. P_{12}	0.906	32.3	-42.8	6.13
2. V_{Area1}^+	0.906	63.0	-45.8	6.63
3. V_{Area2}^+	0.907	42.8	-44.3	6.50
4. I_{Area1}^+	0.904	34.6	-44.4	6.10
5. I_{Area2}^+	0.904	34.5	-43.6	6.06
6. $V_{\varphi Area1} - V_{\varphi Area2}$	0.905	35.0	-45.0	6.15
7. $\frac{V_{M1}+V_{M2}}{2} - \frac{V_{M3}+V_{M4}}{2}$	1.009	66.5	-64.0	32.81
8. $\frac{V_{\varphi M1}+V_{\varphi M2}}{2} - \frac{V_{\varphi M3}+V_{\varphi M4}}{2}$	0.904	32.6	-47.2	5.31

From the results in Table 4.2, the input signals can be further compared. Input signal 8 is the voltage angle difference at machine buses $\left(\frac{V_{\varphi M1}+V_{\varphi M2}}{2} - \frac{V_{\varphi M3}+V_{\varphi M4}}{2}\right)$, it shows the best overall performance. Input signals 2 (V_{Area1}^+) and 3 (V_{Area2}^+) have a slightly longer settling time and a higher overshoot. As a conclusion, all the input signals except input signal 7 $\left(\frac{V_{M1}+V_{M2}}{2} - \frac{V_{M3}+V_{M4}}{2}\right)$, are suitable for damping oscillations.

4.2.2 RT-HIL

In Fig. 4.7-4.8, a comparison of using different input signals from Algorithm 1 when subjected to a small disturbance (Scenario 1), RT-HIL simulation, is shown. The damping provided by all the input signals is highly reduced due to the time delays, scaling and noise. All the input signals perform significantly worse. Thus, it is not possible to discern which signal has the best or worst performance by looking at Fig. 4.7-4.8.

To compare the signals, the same four performance metrics mentioned in Section 4.2.1 are used. Table 4.3 shows that the settling time is much longer for most of the input signals and input signals 2 (V_{Area1}^+), 3 (V_{Area2}^+), 5 (I_{Area2}^+) and 7 $\left(\frac{V_{M1}+V_{M2}}{2} - \frac{V_{M3}+V_{M4}}{2}\right)$ have not damped the oscillations in 20 s. Active power does give the best overall results.

CHAPTER 4. TESTS AND RESULTS

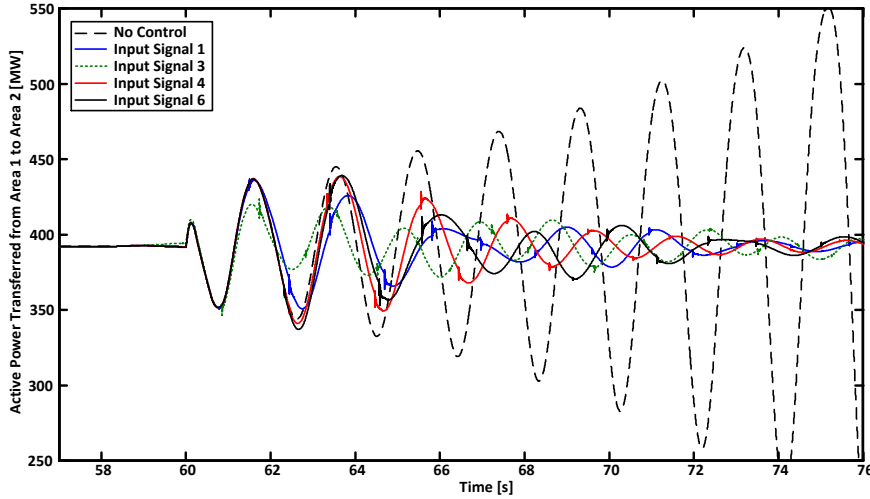


Figure 4.7: Signal selection for RT-HIL simulation using active load control Algorithm 1.

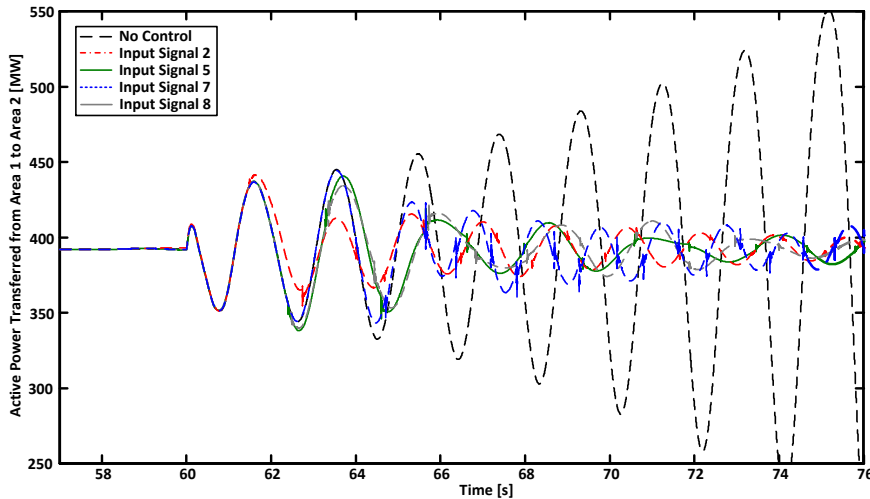


Figure 4.8: Signal selection for RT-HIL simulation using active load control Algorithm 1.

4.3 Further Analysis

4.3.1 Latency Analysis

Even though several factors cause the difference between RT-SIL and RT-HIL simulation results, the main reason is the latency introduced in the HIL setup, that can be understood from the data-flow diagram shown in Fig. 4.9. Time delays have a large impact on power system control loops since the response of the control is

4.3. FURTHER ANALYSIS

Table 4.3: Shows the factors to consider for each input signal in RT-HIL.

Input signal	Decay Ratio	Overshoot [MW]	Undershoot [MW]	Settling Time [s]
1. P_{12}	0.935	44.6	-41.2	12.63
2. V_{Area1}^+	0.951	49.2	-40.8	21.74
3. V_{Area2}^+	0.925	31.5	-45.6	25.88
4. I_{Area1}^+	0.981	46.4	-51.0	14.74
5. I_{Area2}^+	0.959	48.7	-53.9	25.89
6. $V_{\varphi Area1} - V_{\varphi Area2}$	0.945	47.1	-54.9	18.15
7. $\frac{V_{M1}+V_{M2}}{2} - \frac{V_{M3}+V_{M4}}{2}$	0.969	52.4	-48.8	49.80
8. $\frac{V_{\varphi M1}+V_{\varphi M2}}{2} - \frac{V_{\varphi M3}+V_{\varphi M4}}{2}$	0.964	45.0	-52.2	17.32

delayed, which can result in negative contribution towards damping [40]. Because of the latency the phase angle compensation of the load controller has to be modified.

Certain parts of the process have fixed time delays while others have non-deterministic time delays. Extensive analysis have not been done to determine the exact latency in every step of the setup but are intented for future work. The latency due to each part of the HIL setup are discussed next.

1. **Real-Time Simulator:** The real-time simulator has a fixed computation speed of $50\mu s$. The D/A and A/D conversion also has a fixed time.
2. **PMU:** The PMU has a processing delay of 60 ms which includes the A/D conversion and the synchrophasor estimation computation. The PMU also has IEEE C37.118.2 frame formation delay, that is the delay due to the packaging of synchrophasors in IEEE C37.118.2 format. This latency has been estimated to be 45 ms [41].
3. **PDC:** The PDC receives packets from several PMUs but to time align them, it has to wait until all packets for the same time stamp have arrived. The waiting time can vary depending on the geographical location of PMUs and therefore the latency caused by the PDC.
4. **S³DK:** is executed on, a PC with a non real-time operating system, which results in a non-deterministic time delay.
5. **NI-cRIO:** The computation speed of the FPGA was set to $100\mu s$ to avoid overruns because the algorithm was exhausting overall resources of the FPGA.
6. **TCP(Transmission Control Protocol):** This particular communication protocol and communication network has stochastic delay. This delay is though negligible when compared to other latencies mentioned here above.

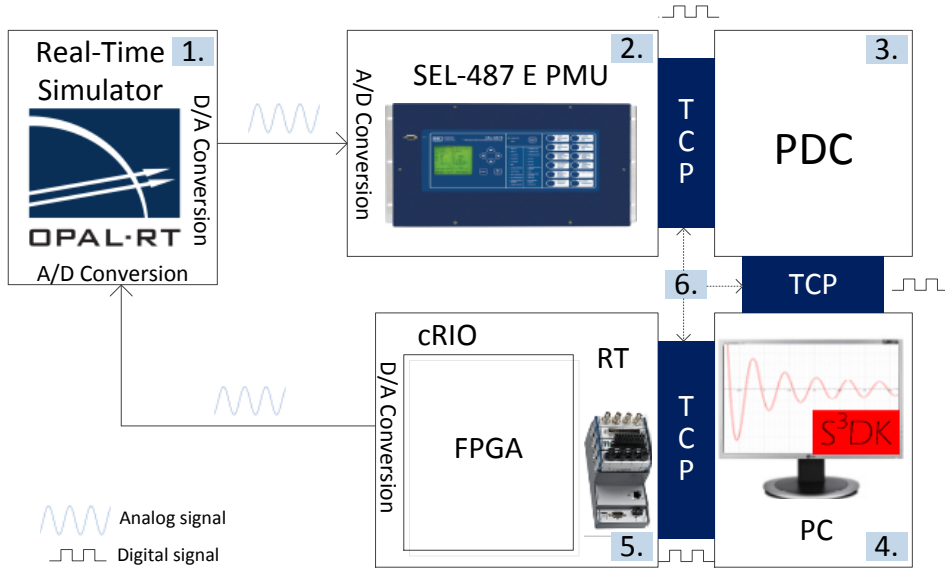


Figure 4.9: The dataflow in the RT-HIL setup.

4.3.2 Scaling Analysis

Another factor that affects the RT-HIL simulation results is the scaling that has to be applied in the RT-HIL setup. When the signal is scaled down, the signal resolution deteriorates and this in turn results in a decrease in signal to noise ratio. In Fig. 4.10, the scaling factor in each step of the setup is shown. Next, each scaling step is explained.

1. A signal sent from the real-time simulator has to be scaled down because of the limit of the analog output listed in Section 2.3.3. Because the low-level input of the PMU is used, the signal has to be within its ± 5 V limit.
2. When the PMU receives the signal through the low-level input it scales it up by multiplying the low-level input signal with a pre-configured CT and VT turn ratio. This scaling can be controlled.
3. The NI-cRIO analog output module has a limit of ± 10 V so the output needs to be scaled down to remain within the output limits of the analog output module.
4. The real-time simulator also has a limit for the analog input that has to be considered, see Section 2.3.3.

4.3. FURTHER ANALYSIS

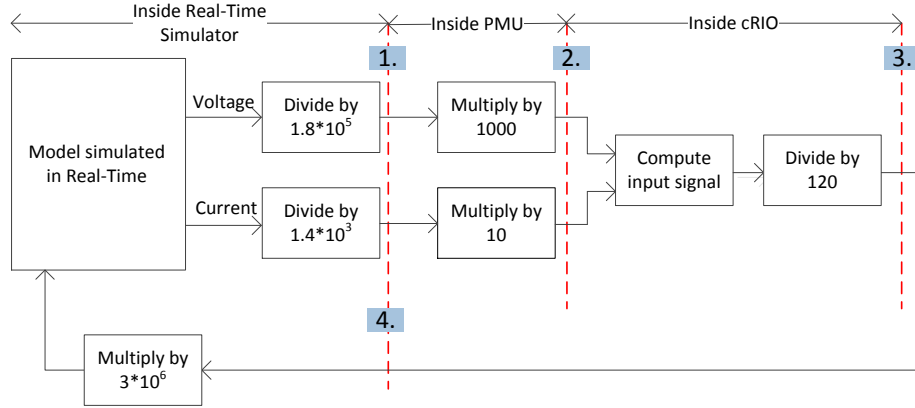


Figure 4.10: Different scaling performed on the signals in the RT-HIL setup.

4.3.3 Noise Analysis

The control signal from the external controller (NI-cRIO) that is fed back to the real-time simulator contains noise. The control signal and a clearer picture of the noise ratio of the signal is shown in Fig. 4.11. The signal received from the controller is low-level because of the output limit of the hardware and has to be scaled up. The control signal after it has been scaled up can be seen in Fig. 4.12 as well as a zoom of the noise. There the noise is in the range of ± 20 kW. Note that the peak output is 121 MW.

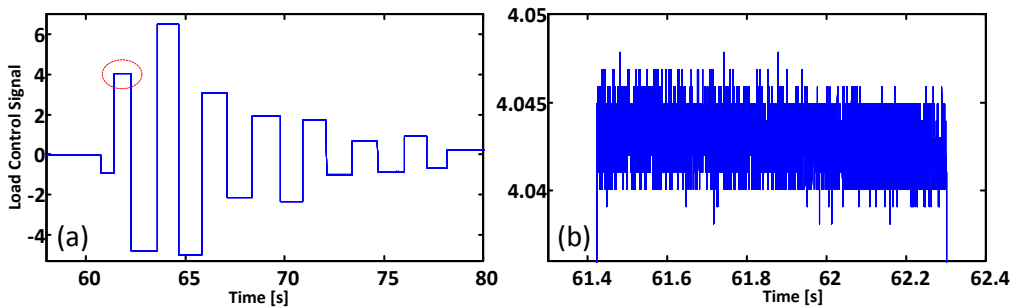


Figure 4.11: (a) The load control signal received from the external controller (NI-cRIO). (b) Zoom in on the noise in the load control signal from the external controller (NI-cRIO).

CHAPTER 4. TESTS AND RESULTS

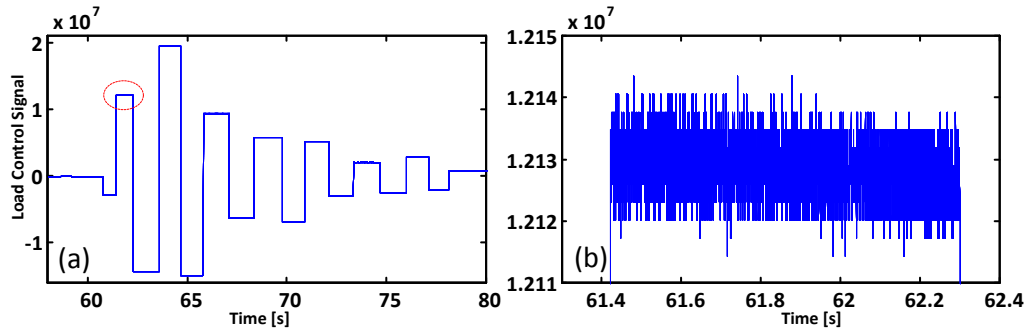


Figure 4.12: (a) The load control signal received from the external controller (NI-cRIO) after being scaled to the appropriate level. (b) Zoom in on the noise in the load control signal from the external controller (NI-cRIO).

Chapter 5

Closure

5.1 Summary

In this thesis load control algorithms for damping of inter-area oscillations were presented. The control algorithms take in synchrophasor measurements as an input signal that can be either local or remote. It uses the phasor-based oscillation damping concept to separate the input signal into its oscillatory content and its average value. Two similar algorithms were presented. Algorithm 1 both increases and sheds the load to provide damping. Algorithm 2 is similar to Algorithm 1, except that it only increases the active power consumption of the load to serve the same function and it disables load-shedding. This algorithm suits TSO requirements, which deem load shedding as undesirable.

To develop the load controller hardware prototype, the V-model development process was used. The development was carried out in two parts. In the first part the design and the software development took place, and in the second part, HIL testing was performed. At the end of the first part of the development, the algorithm was tested using RT-SIL simulation, where both the power system and the control algorithm were simulated in the real-time simulator on separate cores. To test the algorithm in HIL, it was deployed on an external controller (NI-cRIO). It was tested in RT-HIL by simulating the power system on the real-time simulator which feed the load control algorithm with measurements from a PMU. The loop was closed by sending the load modulation signal from the external controller back into the simulator.

Both Algorithm 1 and Algorithm 2 provided damping when executed in RT-SIL and RT-HIL simulation. Algorithm 1 provides quicker damping while Algorithm 2 best suits TSOs requirements. There was a big difference in the simulation results for RT-SIL and RT-HIL due to latencies, noise and scaling in the HIL setup. This resulted in a much slower damping in RT-HIL. Eight different input signals from local and/or remote synchrophasors for the load controller were compared. All eight input signals provided damping, but using voltage magnitude and voltage magnitude difference gave the worst overall results. The user has flexibility to pick

from the other five input signals that include active power, positive sequence current or voltage angle difference to provide damping for this 0.64 Hz inter-area oscillation mode.

5.2 Future Work

There are several directions to extend the breadth and the depth of the work presented in this thesis. Important areas of study are the following.

- **Latency Analysis**

As was discussed in Section 4.3, there are noticeable differences between RT-SIL and RT-HIL simulation results. The latency in the RT-HIL setup is one of the major factors contributing to these differences. Thus, further analysis of the time delay in each step of the setup is needed. Both simulation-based and experimental methods for such analysis can be adopted in further work.

- **SIL and HIL Algorithm Implementation Assessment**

In Section 3.3, the V-model development process was presented. A particular challenge when applying the V-model in this work is the fact that the same programming language and development platform can not be used for developing the SIL and the HIL algorithm. The effect of this difference should be further analysed. Such analysis can be carried out by using the RT-HIL setup to feedback the synchrophasors to the real-time simulator and using them as an input for the SIL algorithm. By comparing these results with the RT-HIL results, the effect of the difference in implementation can be analysed.

- **Enhancement of the Load Control Algorithm**

The load control algorithm presented in this thesis can be further enhanced. One of the approaches to modify the algorithm is presented in Appendix D. Further improvements can also be made to make the algorithm adaptive towards communication latencies and input signal selection. This involves that the algorithm automatically selects the most observable signal as the input signal and calculates the required phase compensation.

- **Design and Testing Multiple Oscillatory Modes and Ambient Load Variations**

Most power systems have multiple oscillatory modes. Therefore the algorithm should be adapted to damp multiple oscillatory modes, both local and inter-area. In addition, the design and testing carried out so far has not considered the effect of ambient load variations, which may impact the performance of the control algorithms.

Bibliography

- [1] D. Wilson, K. Hay, P. McNabb, J. Bialek, Z. Lubosny, N. Gustavsson, and R. Gudmannsson, "Identifying sources of damping issues in the icelandic power system," in *Proc. 16th Power Systems Computation Conf.(PSCC'08)*, 2008.
- [2] J. Vilhjálmsson and F. M. Baldursson, "Þjóðhagslegt gildi uppbyggingar flutningskerfis Landsnets 2013 (The macroeconomic value of building up Landsnets transmission network 2013)." [Online]. Available: <http://www.landsnet.is/landsnet/upplysingatorg/frettir/frett/2013/09/09/Thjodhagslegt-gildi-uppbyggingar-flutningskerfis-Landsnets/>
- [3] P. Kundur, N. J. Balu, and M. G. Lauby, *Power system stability and control*. McGraw-hill New York, 1994, vol. 7.
- [4] D. Wilson, "Landsnets wide area defence scheme design document," 2012, (Not published).
- [5] ——, "Icelandic wide area defence scheme," 2013, (Not published).
- [6] G. I. Valdimarsson, "Aukið Rekstraröryggi Íslenska Raforkukerfisins með Kvíkri Álagsstjórnun Norðuráls (A more secure operation of the Icelandic power system by controling the load consumption at Nordural)," 2013.
- [7] R. H. Park, "Improved reliability of bulk power supply by fast load control", in Proceedings of the 1968, American Power conference, 1968, pp. 445-457.
- [8] I. Kamwa, R. Grondin, et. al., "Large-scale Active-load Modulation for Angle Stability Improvement", IEEE Trans. on Power Systems, Vol. 14, Issue 2, pp. 582-590, May 1999 .
- [9] Raforkutölfræði, "Raforkunotkun, stóriðja, almenningur og skerðanleg notkun (21.11.2013) (load consumption, industrial load, residential load, reducible load)," 2013. [Online]. Available: <http://www.orkustofnun.is/yfirflokkur/raforkutolfraedi/raforkunotkun-storidja-almenningur-og-skerdanlega-notkun>

BIBLIOGRAPHY

- [10] ——, “Raforkunotkun eftir notkunarflokkum (21.11.2013) (load consumption of each user),” 2013. [Online]. Available: <http://www.orkustofnun.is/yfirflokkur/raforkutolfraedi/raforkunotkun-eftir-notkunarflokkum>
- [11] J. Agee, S. Patterson, R. Beaulieu, M. Coultes, R. Grondin, I. Kamwa, G. Trudel, A. Godhwani, R. Bérubé, L. Hajagos *et al.*, “IEEE tutorial course power system stabilization via excitation control,” Tech. Rep., June, Tech. Rep., 2007.
- [12] K. Uhlen, L. Vanfretti, M. de Oliveira, A. Leirbukt, V. Aarstrand, and J. Gjerde, “Wide-Area Power Oscillation Damper implementation and testing in the Norwegian transmission network,” in *Power and Energy Society General Meeting, 2012 IEEE*, July 2012, pp. 1–7.
- [13] K. Uhlen, S. Elenius, I. Norheim, J. Jyrinsalo, J. Elovaara, and E. Lakervi, “Application of linear analysis for stability improvements in the nordic power transmission system,” in *Power Engineering Society General Meeting, 2003, IEEE*, vol. 4, July 2003, pp. –2103 Vol. 4.
- [14] "IEEE Task Force Technical report on Identification of Electromechanical Modes in Power Systems", Special Publication TP462, June, 2012 (PSDP WG Award in 2013).
- [15] N. Chaudhuri, S. Ray, R. Majumder, and B. Chaudhuri, “Interaction between conventional and adaptive phasor power oscillation damping controllers,” in *Power and Energy Society General Meeting, 2010 IEEE*, July 2010, pp. 1–7.
- [16] E. Larsen, J. Sanchez-Gasca, and J. Chow, “Concepts for design of FACTS controllers to damp power swings,” *Power Systems, IEEE Transactions on*, vol. 10, no. 2, pp. 948–956, May 1995.
- [17] A. Heniche and I. Kamwa, “Assessment of Two Methods to Select Wide-Area Signals for Power System Damping Control,” *Power Systems, IEEE Transactions on*, vol. 23, no. 2, pp. 572–581, May 2008.
- [18] ——, “Using measures of controllability and observability for input and output selection,” in *Control Applications, 2002. Proceedings of the 2002 International Conference on*, vol. 2, 2002, pp. 1248–1251 vol.2.
- [19] L. Peng, W. Xiaochen, L. Chao, S. Jinghai, H. Jiong, H. Jingbo, Z. Yong, and A. Xu, “Implementation of CSG’s Wide-Area Damping Control System: Overview and experience,” in *Power Systems Conference and Exposition, 2009. PSCE ’09. IEEE/PES*, March 2009, pp. 1–9.
- [20] “IEEE Standard for Synchrophasor Data Transfer for Power Systems,” *IEEE Std C37.118.2-2011 (Revision of IEEE Std C37.118-2005)*, Dec 2011.

BIBLIOGRAPHY

- [21] "IEEE Standard for Synchrophasor Measurements for Power Systems," *IEEE Std C37.118.1-2011 (Revision of IEEE Std C37.118-2005)*, Dec 2011.
- [22] L. Vanfretti and J. H. Chow, "Synchrophasor Data Applications for Wide-Area Systems," in *17th Power Systems Computation Conference (PSCC), Stockholm, Sweden, 2011*, 2011.
- [23] L. Vanfretti, V. Aarstrand, M. Almas, V. Peric, and J. Gjerde, "A software development toolkit for real-time synchrophasor applications," in *PowerTech (POWERTECH), 2013 IEEE Grenoble*, June 2013, pp. 1–6.
- [24] "eMEGASIM Power Grid Real-Time Digital Hardware in the Loop Simulator." [Online]. Available: <http://www.opal-rt.com/>
- [25] The MathWorks, "Simulink, Simulation and Model Based Design". [Online]. Available: <http://se.mathworks.com/products/simulink>
- [26] The MathWorks, "SimPowerSystems User Guide". [Online]. Available: http://www.mathworks.com/help/releases/R13sp2/pdf_doc/physmod/powersys/powersys.pdf
- [27] M. S. Almas, M. Baudette, L. Vanfretti, S. Lovlund, and J. Gjerde, "Synchrophasor network, laboratory and software applications developed in the STRONG²rid project," in *PES General Meeting/ Conference & Exposition, 2014 IEEE*. IEEE, 2014.
- [28] National Instruments, "Labview, System Design Software". [Online]. Available: <http://www.ni.com/labview/>
- [29] National Instruments, "LabVIEW Real-Time 1 Course Manual", September 2012.
- [30] National Instruments, "LabVIEW FPGA Course Manual", August 2012.
- [31] LabVIEW Online Documentation 'What is Compact RIO'. [Online]. Available: <http://www.ni.com/compactrio/whatis/>
- [32] M. Klein, G. Rogers, and P. Kundur, "A fundamental study of inter-area oscillations in power systems," *Power Systems, IEEE Transactions on*, vol. 6, no. 3, pp. 914–921, Aug 1991.
- [33] L. Angquist and C. Gama, "Damping algorithm based on phasor estimation," in *Power Engineering Society Winter Meeting, 2001. IEEE*, vol. 3, 2001, pp. 1160–1165 vol.3.
- [34] G. M. Jonsdotti, M. S. Almas, M. Baudette, M. Palsson, and L. Vanfretti, "RT-SIL Performance Analysis of Synchrophasor-and-Active Load-Based Power System Damping Controllers," in *IEEE PES GM 2015*, 2015.

BIBLIOGRAPHY

- [35] D. Gianni, A. D'Ambrogio, and A. Tolk, *Modeling and Simulation-Based Systems Engineering Handbook*. CRC Press, 2014.
- [36] I. Kamwa (Hydro-Quebec), "Performance of Three PSS for Interarea Oscillations". [Online]. Available: <http://se.mathworks.com/help/physmod/sps/examples/performance-of-three-pss-for-interarea-oscillations.html>
- [37] "RT-Lab Solo - Getting Started User's Manual, Version 2.11", Centre for Intelligent Machines, McGill University, March 2003. [Online]. Available: http://www.cim.mcgill.ca/ialab/members/usefuldoc/RT-Lab_Instructions_v2.11.pdf
- [38] I. Schweitzer Engineering Laboratories, "SEL-421-4, -5 Relay Protection and Automation System, Instruction Manual," 2014.
- [39] National Instruments, "Operation Instructions and Specifications Compact RIO cRIO-9075/9076." [Online]. Available: <http://www.ni.com/pdf/manuals/375650b.pdf>
- [40] C. Danielson, L. Vanfretti, M. S. Almas, Y. Choompoobutrgool, and J. Gjerde, "Analysis of communication network challenges for synchrophasor-based wide-area applications," in *Bulk Power System Dynamics and Control-IX Optimization, Security and Control of the Emerging Power Grid (IREP), 2013 IREP Symposium*. IEEE, 2013, pp. 1–13.
- [41] M. Almas and L. Vanfretti, "RT-HIL Implementation of Hybrid Synchrophasor and GOOSE-based Passive Islanding Schemes."

Appendix A

Test Power System Model Parameters

Here are the parameters for the test power system model presented in Section 3.1. The common parameters for the four synchronous generators in the system are given here below in p.u. on the generator base, similar to [32].

$$R_s = 0.0025 \quad X_d = 1.8 \quad X_q = 1.7 \quad (\text{A.1})$$

$$X_l = 0.2 \quad X'_d = 0.3 \quad X'_q = 0.55 \quad (\text{A.2})$$

$$X''_d = X''_q = 0.25 \quad R_s = 0.0025 \quad X_q = 1.7 \quad (\text{A.3})$$

$$(\text{A.4})$$

$$\begin{aligned} R_s &= 0.0025 & X_d &= 1.8 & X_q &= 1.7 & X_l &= 0.2 & X'_d &= 0.3 & X'_q &= 0.55 & X''_d &= X''_q &= 0.25 \\ R_s &= 0.0025 & X_d &= 1.8 & X_q &= 1.7 & X_l &= 0.2 & X'_d &= 0.3 & X'_q &= 0.55 & X''_d &= X''_q &= 0.25 \\ T'_{do} &= 8s & T'_{qo} &= 0.4s & T''_{do} &= 0.03s & T''_{qo} &= 0.05s \end{aligned}$$

The step up transformer impedance is $0 + j0.15$ and the transmission line parameters are the following:

$$r = 0.0001 \text{ pu/km}, \quad x_l = 0.001 \text{ pu/km}, \quad b_c = 0.00175 \text{ pu/km}, \quad \text{Nominal Voltage} = 230 \text{ kV}.$$

The excitation parameters that are common for all generators are:

$$K_A = 200 \quad T_A = 0.001 \quad T_r = 0.02 \quad T_C = T_B = 0$$

Appendix B

Results for Scenario 2

Figure B.1 compares RT-SIL simulation results using different input signals for Algorithm 1 when Scenario 2 occurs. In this case not all eight input signals were able to damp the oscillations, that is input signal 3 (V_{Area2}^+) and 7 ($\frac{\bar{V}_{M1}+V_{M2}}{2} - \frac{V_{M3}+V_{M4}}{2}$) and are therefore not provided for Scenario 2. The other six input signals provide adequate damping within 12 s after the fault.

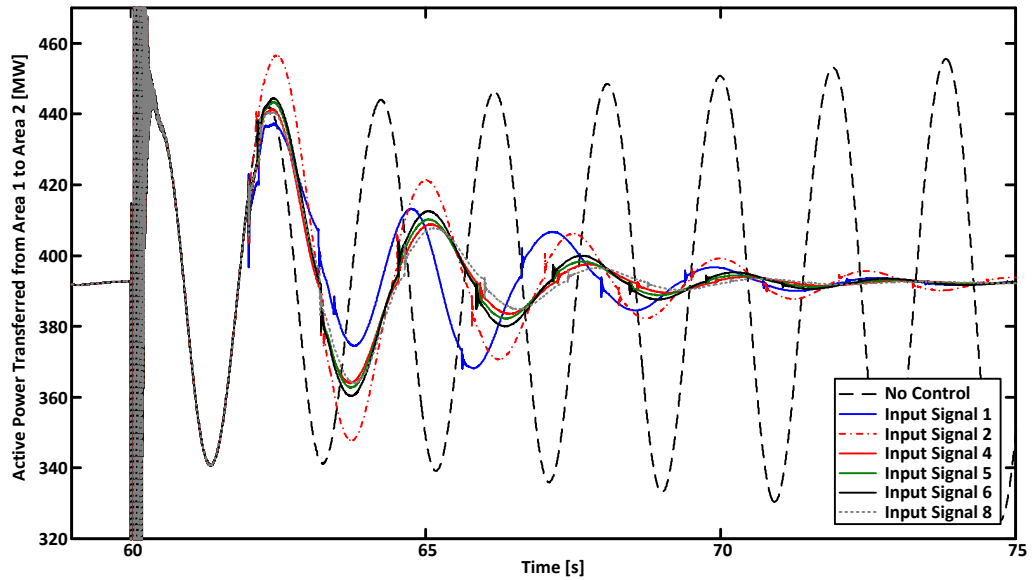


Figure B.1: Signal selection for RT-SIL simulation using active load control Algorithm 1, Scenario 2.

APPENDIX B. RESULTS FOR SCENARIO 2

To compare the signals we use the performance metrics listed in Section 4.2.1 are used and there results are listed in Table B.1. Input signal 8 ($\frac{V_{\varphi M1}+V_{\varphi M2}}{2} - \frac{V_{\varphi M3}+V_{\varphi M4}}{2}$) as for Scenario 1 shows the best overall performance, while input signal 2 (V_{Area1}^+) has the longest settling time and the largest overshoot.

Table B.1: Shows the four factors considered for each input signal when RT-SIL simulation is used, in case of Scenario 2.

Input signal	Decay Ratio	Overshoot [MW]	Undershoot [MW]	Settling Time [s]
1. P_{12}	0.920	45.3	-51.4	10.11
2. V_{Area1}^+	0.919	64.7	-51.4	11.44
3. V_{Area2}^+	x	x	x	x
4. I_{Area1}^+	0.899	49.4	-51.4	8.08
5. I_{Area2}^+	0.901	51.5	-51.4	8.04
6. $V_{\varphi Area1} - V_{\varphi Area2}$	0.905	52.6	-51.4	9.17
7. $\frac{V_{M1}+V_{M2}}{2} - \frac{V_{M3}+V_{M4}}{2}$	x	x	x	x
8. $\frac{V_{\varphi M1}+V_{\varphi M2}}{2} - \frac{V_{\varphi M3}+V_{\varphi M4}}{2}$	0.897	48.6	-51.4	7.78

Appendix C

Figures of Setup



Figure C.1: Shows the SmarTS Lab setup. Highlighted are the devices used for the experiments in this thesis. (1. OPAL Real-Time Simulator, 2. SEL PMUs, 3. PDC Interface, 4. cRIO rack)

APPENDIX C. FIGURES OF SETUP

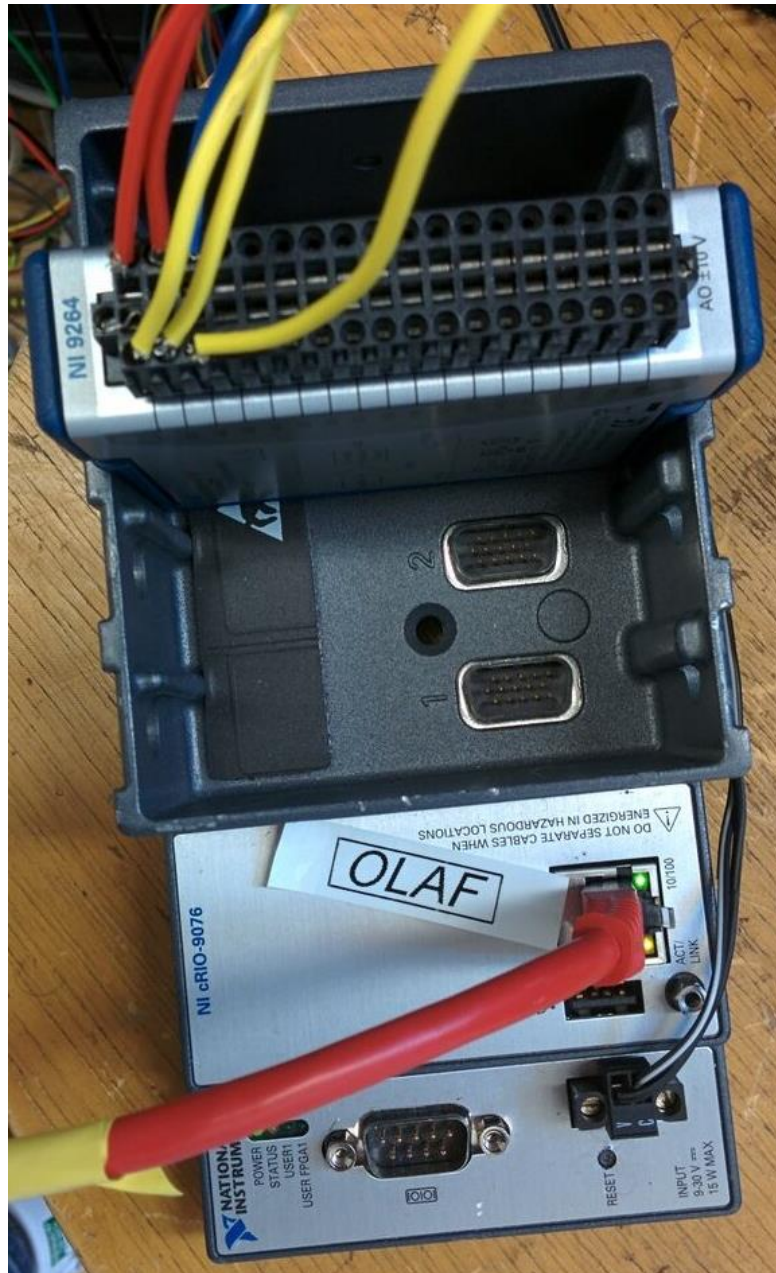


Figure C.2: NI-cRIO-9076 with NI 9264 AO module mounted in the chassis.

Appendix D

New Approach for Determining the Amount of Load Change

Because of the limitations of the active load control algorithms presented in this thesis, other options were explored. One of them that has shown promising results in RT-SIL simulation, which are briefly presented here. Extensive experiments have not been performed to test this approach because of time constraints, but in future work on load control for oscillation damping, it is worth considering this approach.

This new approach exploits the fact that the peak of a sine-wave can be estimated before the peak is reached. In this case the active power oscillation can be expressed as a sine-wave with the following equation.

$$f(t) = P_{max} \sin(\omega_1 t) \quad (\text{D.1})$$

where P_{max} is the maximum value the sine-wave will reach, ω_1 is the frequency of oscillation and t is the time. At a certain time Δt :

$$f(\Delta t) = P_{max} \sin(\omega_1 \Delta t) = \Delta P \quad (\text{D.2})$$

the value of ΔP and Δt can be measured and since ω_1 is known the value of P_{max} can be found:

$$P_{max} = \frac{\Delta P}{\sin(\omega_1 \Delta t)} \quad (\text{D.3})$$

This can also be seen graphically in Fig. D.1

Figure D.2 shows the calculation of P_{max} implemented in MATLAB/SIMULINK. Below, the steps taken in the code are explained.

1. Take the oscillatory content of the active power and determine when it becomes positive. At that moment start a counter.
2. Take the oscillatory content of the active power and determine when it becomes negative. At that moment start a counter.

APPENDIX D. NEW APPROACH FOR DETERMINING THE AMOUNT OF LOAD CHANGE

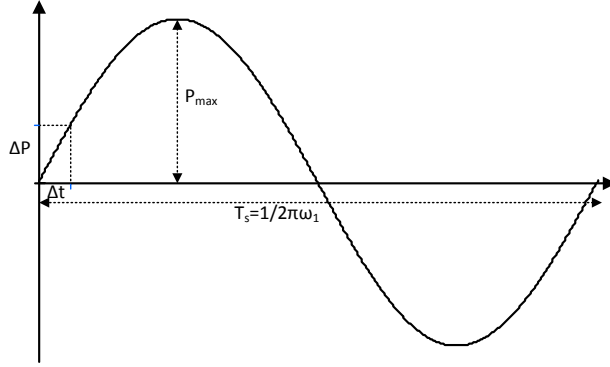


Figure D.1: A graphical explanation to indicate how P_{max} can be estimated.

3. Determine when the time since the oscillatory content of the active power crossed zero becomes $\Delta t = 0.1$ s.
4. Calculate the lower part of the derivative in equation (D.3), that is $\sin(\omega_1 \Delta t)$.
5. Estimate ΔP at time $\Delta t = 0.1$ s.
6. Calculate P_{max} using equation (D.3).

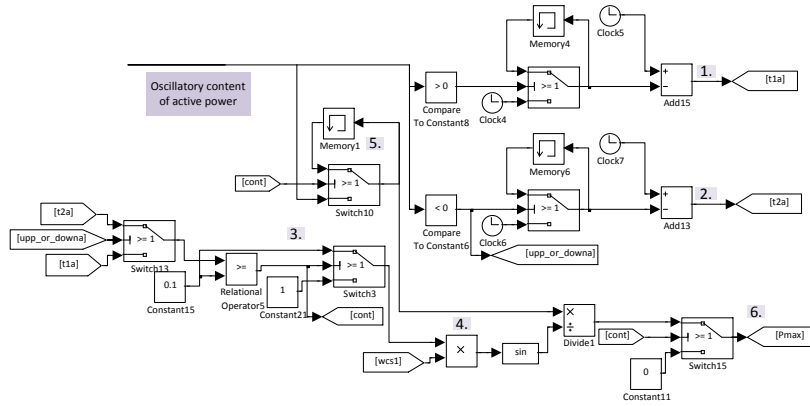


Figure D.2: Shows the Simulink model for determining P_{max} .

In Fig. D.3, the oscillatory content of the active power and the P_{max} estimate made by the algorithm in Fig. D.2 are shown. The oscillations are caused by Scenario 1 and the new algorithm is applied to damp the oscillations.

The advantage of estimating the P_{max} value before hand is that this value can be applied to increase and decrease the load instead of scaling the different inputs. In Fig. D.4 and D.5 the new approach is compared to active load control Algorithm 1 for input signal 1 (P_{12}) and input signal 8 ($\frac{V_{\varphi M1}+V_{\varphi M2}}{2} - \frac{V_{\varphi M3}+V_{\varphi M4}}{2}$) for a small disturbance (Scenario 1). In both cases the new approach damps the oscillations quicker.

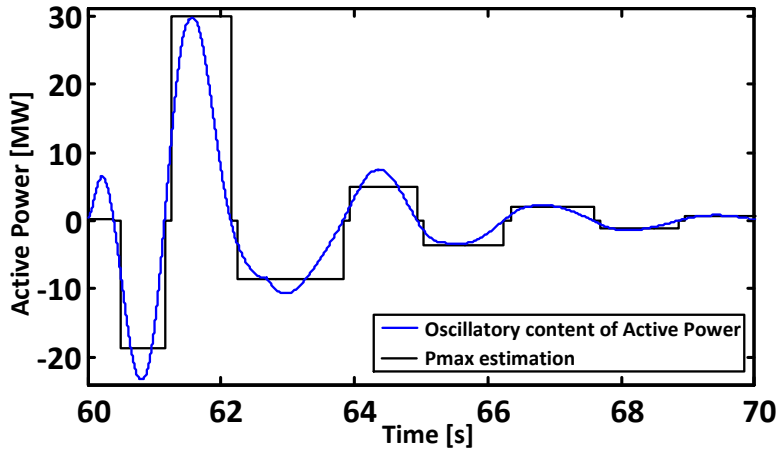


Figure D.3: The estimated value of P_{max} as calculated with the algorithm compared to the actual active power signal.

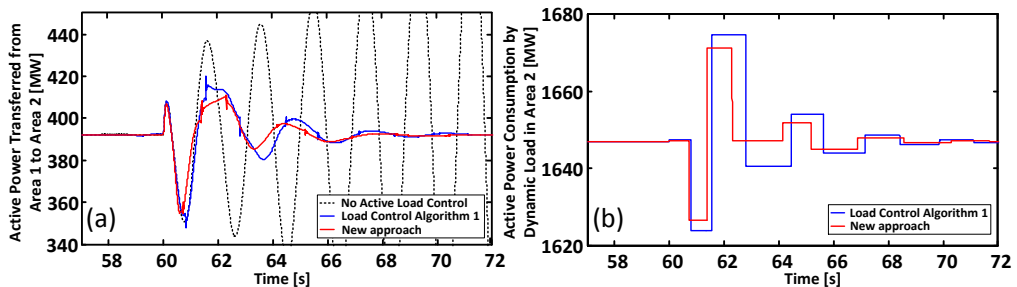


Figure D.4: A comparison of the load control Algorithm 1 presented in the thesis and the new approach when subjected to small disturbance (Scenario 1). Input signal 1 (P_{12}) is used.

APPENDIX D. NEW APPROACH FOR DETERMINING THE AMOUNT OF LOAD CHANGE

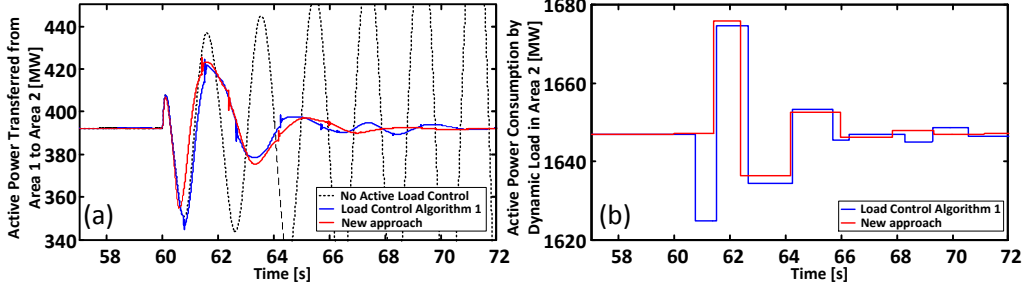


Figure D.5: A comparison of the load control Algorithm 1 presented in the thesis and the new approach when subjected to small disturbance (Scenario 1). Input signal 8 ($\frac{V_{\varphi M1}+V_{\varphi M2}}{2} - \frac{V_{\varphi M3}+V_{\varphi M4}}{2}$) is used.